Modelling and investigation of the CD4+ T cells-macrophages paradox in melanoma immunotherapies

Eftimie, Raluca; Hamam, Haneen

Published in:
Journal of Theoretical Biology

DOI:
10.1016/j.jtbi.2017.02.022

Publication date:
2017

Document Version
Publisher's PDF, also known as Version of record

Journal of Theoretical Biology 420 (2017) 82–104

Contents lists available at ScienceDirect

Journal of Theoretical Biology

journal homepage: www.elsevier.com/locate/yjtbi

Modelling and investigation of the $CD4^+$ T cells – Macrophages paradox in melanoma immunotherapies

Raluca Eftimie*, Haneen Hamam

Division of Mathematics, University of Dundee, Dundee DD1 4HN, United Kingdom

ARTICLE INFO

MSC:
92C50
34A34

Keywords:
M1 and M2 macrophages
Th1 and Th2 immune cells
B16 melanoma
Mathematical approach

ABSTRACT

It is generally accepted that tumour cells can be eliminated by M1 anti-tumour macrophages and $CD8^+$ T cells. However, experimental results over the past 10–15 years have shown that B16 mouse melanoma cells can be eliminated by the $CD4^+$ T cells alone (either Th1 or Th2 sub-types), in the absence of $CD8^+$ T cells. In some studies, elimination of B16 melanoma was associated with a Th1 immune response (i.e., elimination occurred in the presence of cytokines produced by Th1 cells), while in other studies melanoma elimination was associated with a Th2 immune response (i.e., elimination occurred in the presence of cytokines produced by Th2 cells). Moreover, macrophages have been shown to be present inside the tumours, during both Th1 and Th2 immune responses. To investigate the possible biological mechanisms behind these apparently contradictory results, we develop a class of mathematical models for the dynamics of Th1 and Th2 cells, and M1 and M2 macrophages in the presence/absence of tumour cells. Using this mathematical model, we show that depending on the re-polarisation rates between M1 and M2 macrophages, we obtain tumour elimination in the presence of a type-I immune response (i.e., more Th1 and M1 cells, compared to the Th2 and M2 cells), or in the presence of a type-II immune response (i.e., more Th2 and M2 cells). Moreover, tumour elimination is also possible in the presence of a mixed type-I/type-II immune response. Tumour growth always occurs in the presence of a type-II immune response, as observed experimentally. Finally, tumour dormancy is the result of a delicate balance between the pro-tumour effects of M2 cells and the anti-tumour effects of M1 and Th1 cells.

1. Introduction

The anti-tumour role of the immune system has been documented for at least a century, with one of the earliest studies on the role of immune surveillance against transformed cells being published by Ehrich (1909). The last 20–30 years have seen a very rapid increase in the number of experimental studies that investigate the molecular and cellular mechanisms behind the tumour-immune interactions. However, in many cases, the experimental results are contradictory. For example, Mattes et al. (2003) investigated the anti-tumour effects of two types of $CD4^+$ T cells (Th1 and Th2 cells) on B16 melanoma, and concluded that contrary to the generally accepted idea that the $CD4^+$ T cells have only a helper role, they can actually eliminate tumours on their own via the cytokines they produce. Moreover, the authors showed that while the Th1-tumour interactions led to temporary tumour control followed by tumour escape and growth (see Fig. 1(a)), the Th2-tumour interactions led in the long term to tumour elimination (see Fig. 1(a)). In fact, Mattes et al. (2003) suggested that tumour elimination in the presence of Th2 cells is helped by the influx of eosinophils to the tumour site. In addition to eosinophils, the authors also showed the presence of tumour-infiltrating macrophages (see Fig. 1(b)), which seemed to be associated with tumour growth (but the authors did not investigate the possible anti-tumour/pro-tumour action of these macrophages). In a later study, Xie et al. (2010) showed that the Th1 cells can actually eliminate B16 melanoma cells (see Fig. 2(a)). Kobayashi et al. (1998) showed that the growth of B16F10 cells is associated with a large number of Th2 cells and a high concentration of IL-4 cytokines (see Fig. 2(b)). Moreover, Chen et al. (2011) showed that the growth of B16 melanoma cells is associated with a shift from anti-tumour M1 macrophages to pro-tumour M2 macrophages (see Fig. 2(c)). (Note that the classification of macrophages into M1 and M2 phenotypes mirrors the Th1 and Th2 nomenclature (Mantovani et al., 2008), and despite this strict classification there is actually a continuum of phenotypes between the M1 and M2 extremes).

The anti-tumour effects of Th1 and Th2 cells are exerted by the cytokines they produce: (i) the Th1 cells produce type-I cytokines, such as IFN–γ, IL–2, TNF–α and TNF–β (Magombedze et al., 2014; Lucey

* Corresponding author.
E-mail address: r.a.eftimie@dundee.ac.uk (R. Eftimie).

http://dx.doi.org/10.1016/j.jtbi.2017.02.022
Received 14 February 2016; Received in revised form 12 February 2017; Accepted 16 February 2017
Available online 20 February 2017

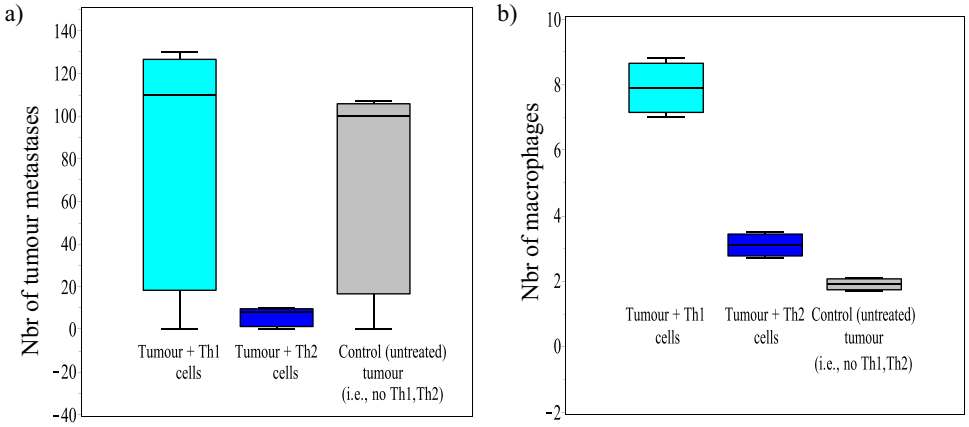

Fig. 1. Data approximated and re-drawn from Mattes et al. (2003), where the authors transfer Th1 cells or Th2 cells into C57BL/6 mice that were previously injected with B16-OVA melanoma cells. a) Number of tumour metastases after the adoptive transfer of Th1 cells, Th2 cells and for the control case (i.e. no treatment with immune cells). b) Number of tumour-infiltrating macrophages following the adoptive transfer of Th1 cells and Th2 cells, and comparison with the number of macrophages in control tumours (with no adoptive transfer of Th1/Th2 cells).

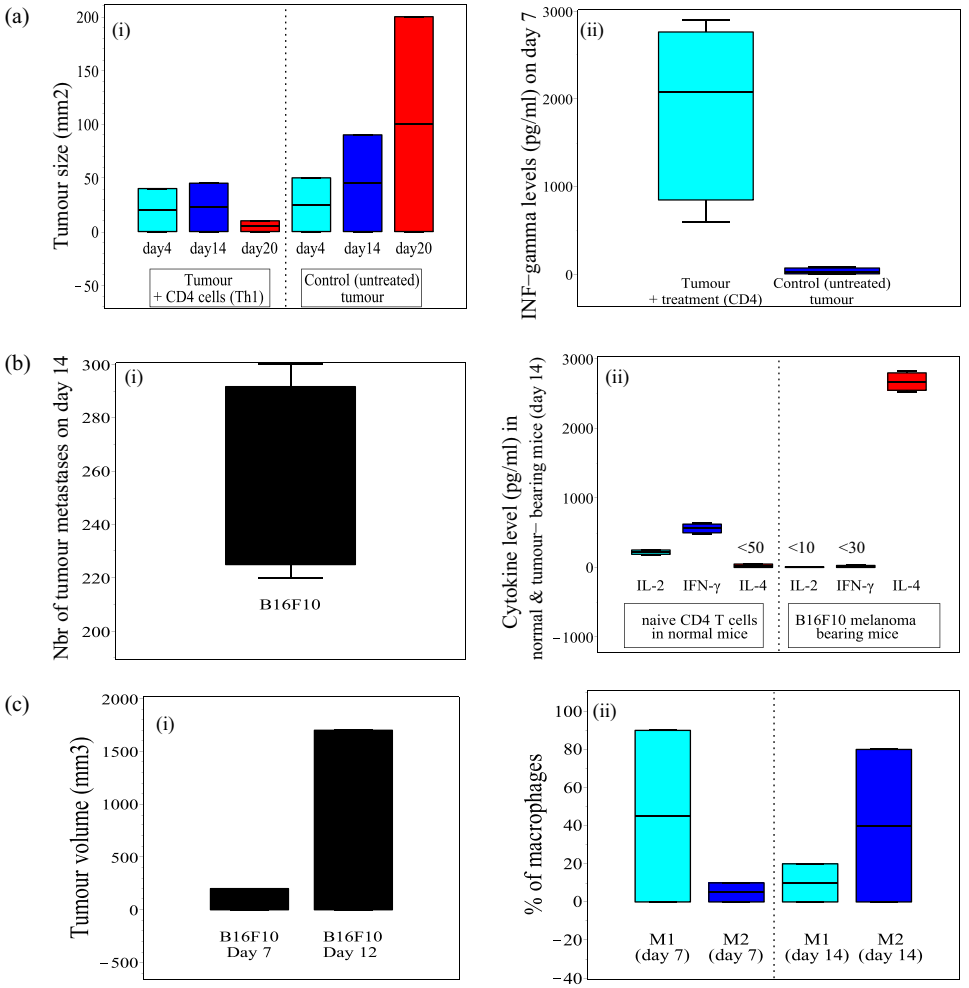

Fig. 2. (a) Data approximated and re-drawn from Xie et al. (2010), where the authors inject RAG$^{-/-}$ mice (which do not have any CD8$^+$ T cells, B cells or NKT cells) with B16F10 melanoma cells. Panel (i) shows tumour size on day 20 for mice injected with CD4$^+$ T cells and for control mice (with no injection of CD4$^+$ T cells); Panel (ii) shows the level of IFN-γ in mice injected with CD4$^+$ T cells and in control mice, suggesting that the CD4$^+$ T cells that reduce the size of the tumour are actually Th1 cells (which produce high levels of IFN-γ). (b) Data approximated and re-drawn from Kobayashi et al. (1998), where the authors inject C57BL/6 mice with B16F10 melanoma cells. Panel (i) shows the number of metastatic colonies on day 14 after injection; Panel (ii) shows the level of IL −2 IFN-γ and IL −4 cytokines produced by naive CD4$^+$ T cells in normal mice and in mice injected with B16F10 cells. (c) Data approximated and re-drawn from Chen et al. (2011), where the authors inject C57BL/6 mice with B16F10 melanoma cells. Panel (i) shows tumour volume on days 7 and 12 after transfer of tumour cells; Panel (ii) shows the percentage of M1 and M2 macrophages inside the tumour, on days 7 and 14.

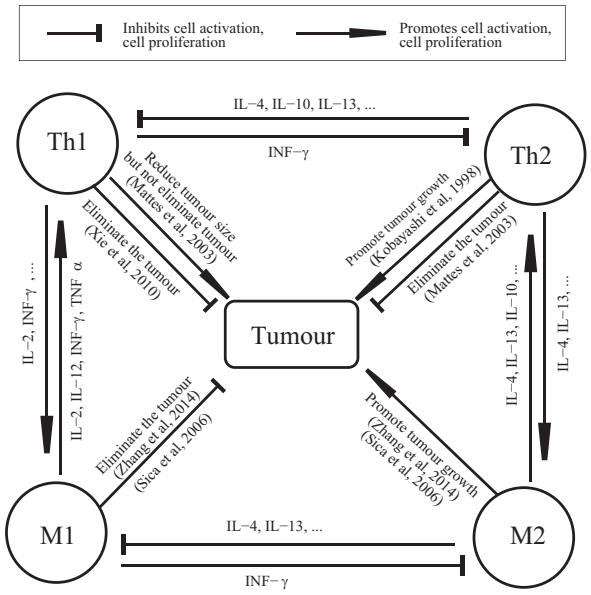

Fig. 3. Graphical description of the possible interactions between M1/M2 macrophages, Th1/Th2 cells and tumour cells, via type-I cytokines (e.g. IFN $-\gamma$) and type-II cytokines (e.g. IL −4, IL −13).

et al., 1996); (ii) the Th2 cells produce type-II cytokines, such as IL−4, IL−5, IL−6, IL−10 and IL−13 Romagnani (1999); Lucey et al. (1996). It is usually thought that the type-I cytokines (e.g., IFN-γ, IL−2) have an anti-tumour role (Lucey et al., 1996), while the type-II cytokines (e.g., IL−10) are generally associated with tumour growth (Lucey et al., 1996). These cytokines are not only produced by the Th1/Th2 cells, but also by other cells in the environment: e.g., macrophages, neutrophils, eosinophils, etc. (Lucey et al., 1996). In particular, the macrophages can produce, and respond to, both type-I and type-II cytokines. Classically activated M1 macrophages are induced by cytokines such as IFN−γ or TNF−α (Mantovani et al., 2008). Alternatively activated M2 macrophages are induced by cytokines such as IL−4 and IL−13 (Mantovani et al., 2008). Moreover, the M1 cells are associated with Th1 responses, being involved in resistance against tumours (Mantovani et al., 2008). On the other hand, the M2 cells are associated with Th2 responses, being involved in tumour progression, tissue repair and remodelling (Mantovani et al., 2008). We emphasise here the crosstalk between the Th cells and macrophages via the type-I and type-II cytokines, which might influence the tumour microenvironment (see also Fig. 3).

The goal of this study is to derive a class of mathematical models that can propose hypotheses regarding the apparent paradoxical results in the anti-tumour effects of Th1 and Th2 cells, and M1 and M2 macrophages. We note that in the mathematical literature there are various models investigating different aspects of the interactions between Th1 and Th2 cells, and between M1 and M2 macrophages. For example, the Th1-Th2 dynamics was investigated in the context of cell differentiation and cross-regulation (Yates et al., 2000; Bergmann et al., 2001; Fishman and Perelson, 1999), during the immune response to allergens (Gross et al., 2011) and asthma development (Kim et al., 2013), during autoimmune diseases (Louzoun et al., 2001), following T cell vaccination (Severins et al., 2008), during bacterial infection in ruminants (Magombedze et al., 2014), or in the rejection of cancers such as melanoma (Eftimie et al., 2010; Kogan et al., 2013). The M1-M2 dynamics was investigated during macrophage activation post-myocardian infarction (Wang et al., 2012), during wound healing (Yu, 2014), or in the rejection of pancreatic cancer (Louzoun et al., 2014). However, very few mathematical models investigate the interplay between M1/M2 macrophages and Th1/Th2 cells during cancer evolution (den Breems and Eftimie, 2016). For example, the study in den Breems and Eftimie (2016) investigated (numerically and with the help of sensitivity analysis) the influence of the ratio of M1 and M2 macrophages on early and advanced tumour growth, for normal and mutated tumour cells. The authors showed that their model can only exhibit tumour growth (i.e., no tumour elimination). Moreover, they showed that while a ratio of M2:M1>1 can always predict growth towards tumour carrying capacity, a ratio of M2:M1<1 can lead to either growth towards carrying capacity or growth towards a lower tumour size.

In this study, we will investigate the possible mechanisms that could explain the elimination of B16 melanoma by Th2 cells in Mattes et al. (2003) and by Th1 cells in Xie et al. (2010), and the role played by M1 and M2 macrophages in tumour growth and elimination (given the crosstalk between Th1/Th2 cells and M1/M2 cells via the cytokines they produce; see Fig. 3). To this end we develop two mathematical models: (i) a model for the interactions between the Th cells and macrophages alone, which is used to investigate the type-I and type-II immune responses they generate (where we define a *type-I immune response* to be the response dominated by Th1 and M1 cells, and a *type-II immune response* to be the response dominated by Th2 and M2 cells); (ii) a model for the interactions between tumour cells, Th cells and macrophages. We show that tumour can be eliminated both in the presence of a type-I immune response and a type-II immune response. Tumour growth is always associated with the presence of a type-II immune response.

The structure of this article is as follows. In Section 2 we introduce a mathematical model for the Th cells-macrophages interactions and discuss the long-term behaviour of the model by investigating the number and stability of the steady states. We also investigate numerically the dynamics of this model, and discuss the conditions under which the model displays a type-I or a type-II immune response. In Section 3 we generalise the previous model to incorporate also tumour dynamics. Again, we calculate the steady states and their stability to emphasise the complexity of the new model. We also investigate numerically the short-term and long-term dynamics of the model for tumour-immune interactions, and discuss the parameter values for which we see tumour elimination in the presence of a type-I immune response and in the presence of a type-II immune response. We conclude in Section 3.3 with a summary and discussion of the results.

2. Modelling the Th1 & Th2 and M1 & M2 interactions

We first ignore the presence of the tumour, and investigate the dynamics of the interactions between the Th cells and macrophages, following their cross-talk (via cytokines, which we consider implicitly). Thus we define four variables: the density of Th1 cells (H_1), the density of Th2 cells (H_2), the density of M1 macrophages (M_1) and the density of M2 macrophages (M_2). The time-evolution of these variables is given by

$$\frac{dH_1}{dt} = a_{H_1}M_1 + p_{H_1}H_1M_1\left(1 - \frac{H_1+H_2}{m_1}\right) - e_{H_1}H_1, \tag{1a}$$

$$\frac{dH_2}{dt} = a_{H_2}M_2 + p_{H_2}H_2M_2\left(1 - \frac{H_1+H_2}{m_1}\right) - e_{H_2}H_2, \tag{1b}$$

$$\frac{dM_1}{dt} = a_{M_1}H_1 + p_{M_1}M_1\left(1 - \frac{M_1+M_2}{m_2}\right) - e_{M_1}M_1 + r_{M_1}M_2 - r_{M_2}M_1, \tag{1c}$$

$$\frac{dM_2}{dt} = a_{M_2}H_2 + p_{M_2}M_2H_2\left(1 - \frac{M_1+M_2}{m_2}\right) - e_{M_2}M_2 - r_{M_1}M_2 + r_{M_2}M_1. \tag{1d}$$

The following assumptions are incorporated in Eqs. (1):

- The Th1 cells are activated at a rate a_{H_1} in the presence of IFN-γ cytokines that can be produced by M1 macrophages (Preuße et al.,

2012). These cells grow at a rate p_{H_1} in the presence of type-I cytokines such as IL −2 (Taylor-Robinson, 1997) or IL −12 (His et al., 1993) (which can be also produced by M1 macrophages), up to maximum carrying capacity m_1. The growth term also incorporates the competition between the Th1 and Th2 cells for antigens (Magombedze et al., 2014). Note that high Th2 responses lead to a suppression of Th1 responses and vice-versa, as observed experimentally (Magombedze et al., 2014). The natural death rate of Th1 cells is e_{H_1} (Magombedze et al., 2014).

- The Th2 cells are activated at a rate a_{H_2} in the presence of IL −4 and IL −13 cytokines that can be produced by M2 macrophages (Romagnani, 1999). Moreover, the Th2 cells grow at a rate p_{H_2} in the presence of IL −4 (Zhu et al., 2002), up to maximum carrying capacity m_1. The natural death rate of Th2 cells is e_{H_2} (Magombedze et al., 2014).
- The M1 macrophages are activated at a rate a_{M_1} in the presence of IFN $-\gamma$ cytokine, produced also by Th1 cells (Preuße et al., 2012; Weisser et al., 2013). Also, the M1 cells grow at a rate p_{M_1} via a self renewal process (Helming, 2011), up to a maximum carrying capacity m_2. The apoptosis rate of M_1 cells is e_{M_1} (Gauthier et al., 2013). Note that M1 macrophages can become M2 macrophages, in the presence of type-II cytokines (Allavena and Mantovani, 2012). We denote by r_{M_1} the re-polarisation rate from M1 to M2 macrophages (Wang et al., 2012).
- The M2 macrophages are activated at a rate a_{M_2} in the presence of IL −4, IL −13 (which can be produced by Th2 cells) (Weisser et al., 2013). Moreover, the M2 cells proliferate in the presence of IL −4 cytokines characteristic to a Th2-environment (Jenkins et al., 2011) (hence the proliferation rate $p_{M_2}H_2$), up to a maximum carrying capacity of m_2 cells. (Note that, in contrast to the M2 cells, the M1 cells proliferate via self-renewal (Helming, 2011), and thus we do not multiply the p_{M_1} rate with the H_1 variable.) The apoptosis rate of M2 cells is e_{M_2} (Gauthier et al., 2013). Finally, since the M2 macrophages can change their phenotype and become M1 macrophages in the presence of type-I cytokines (Allavena and Mantovani, 2012), we denote by r_{M_2} the re-polarisation rate from M2 to M1 cells (Wang et al., 2012).

We note here that there are a few studies that suggest the possibility of Th1 ↔ Th2 re-polarisation based on the environment (Panzer et al., 2011). However, since this concept of Th re-polarisation is still new, we will not investigate it in this study.

A non-dimensionalised version of the model (1) is shown in Appendix C. However, throughout this study we prefer to work with this dimensional model since in the next two sections we will discuss some of the results in the context of dimensional experimental studies. Moreover, the non-dimensionalisation approach does not reduce significantly the number of model parameters.

2.1. Steady state and stability

Before investigating the long-term behaviour of model (1), we mention that this system has non-negative solutions provided that the initial data are also non-negative (see the discussion in Appendix B). A first step in analysing the long-term dynamics of (1) is to focus on the steady states. The analysis illustrates two types of equilibria:

1. No immune cells: $(H_1^*, H_2^*, M_1^*, M_2^*) = (0, 0, 0, 0)$. For the parameter values used throughout this study (see Table A.1, and the discussion in Appendix E), the eigenvalues of the Jacobian matrix associated with system (1) are negative at this steady states (see Fig. E.16 in Appendix E). Thus, for these parameter values, this immune-free state is stable. A more general discussion about the conditions on the parameter values that allow for stable or unstable zero states can be found in Appendix E.
2. All immune cells present: $(H_1, H_2, M_1, M_2) = (H_1^*, H_2^*, M_1^*, M_2^*)$. There are two such equilibrium points, where the states H_1^*, H_2^*, M_1^* and M_2^* are given implicitly by the following equations:

$$M_1^* = \frac{e_{H_1}H_1^*}{a_{H_1} + p_{H_1}H_1^*\left(1 - \frac{H_1^* + H_2^*}{m1}\right)}, \tag{2a}$$

$$H_1^* = \frac{e_{M_1}M_1^* + r_{M_2}M_1^* - r_{M_1}M_2^* - p_{M_1}M_1^*\left(1 - \frac{M_2^* + M_1^*}{m_2}\right)}{a_{M_1}}, \tag{2b}$$

$$M_2^* = \frac{e_{H_2}H_2^*}{a_{H_2} + p_{H_2}H_2^*\left(1 - \frac{H1^* + H_2^*}{m1}\right)}, \tag{2c}$$

$$H_2^* = \frac{e_{M_2}M_2^* + r_{M_1}M_2^* - r_{M_2}M_1^*}{a_{M_2} + p_{M_2}M_2^*\left(1 - \frac{M_2^* + M_1^*}{m_2}\right)}. \tag{2d}$$

For the parameter values chosen in Table A.1, Fig. 4 shows that there are two non-zero steady states (and simple linear stability analysis indicates that one state is stable while the other state is unstable - see Fig. E.16 in Appendix E). Moreover, for the parameter values used here, we observe that $M_1^* > M_2^*$, and correspondingly $H_1^* > H_2^*$ (see also the caption of Fig. 4 for the exact steady state values). This corresponds to a type-I immune response that dominates the dynamics of model (1).

To investigate the possibility of having also other types of immune responses that dominate the dynamics (i.e., a type-II response where $M_1^* < M_2^*$ and $H_1^* < H_2^*$; or a mixed type-I/type-II response where, for example, $M_1^* > M_2^*$ but $H_1^* < H_2^*$) in Fig. 5 we present a bifurcation diagram for the ratio of M_1^*/M_2^* and H_1^*/H_2^* steady states (given by Eqs. (2)), as we vary: (a) the ratio of macrophages re-polarisation rates (r_{M_1}/r_{M_2}) versus the ratio of activation rates for the Th1 and Th2 cells (a_{H_1}/a_{H_2}), and (b) the ratio of macrophages re-polarisation rates (r_{M_1}/r_{M_2}) versus the ratio of macrophage activation rates (a_{M_1}/a_{M_2}). When we vary a_{H_1}/a_{H_2} in panel (a), we notice that we can have:

- a type-I immune response at the overlap between the red (gray on black/white print) surfaces, when $r_{M_1}/r_{M_2} \gg 1$ and $a_{H_1}/a_{H_2} \leq 1$;
- a type-II immune response (at the overlap between the blue surfaces) when $r_{M_1}/r_{M_2} \ll 1$;
- a mixed type-I/type-II immune response when $r_{M_1}/r_{M_2} \geq 1$ and $a_{H_1}/a_{H_2} \ll 1$.

When we vary a_{M_1}/a_{M_2} in panel (b), we notice that we can have either a type-I or a type-II immune response (since the curves for M_1^*/M_2^* and H_1^*/H_2^* overlap). Details of how we created these bifurcation diagrams are presented in Appendix D.

2.2. Short- and long-term immune dynamics

To investigate numerically the transient and long-term dynamics of macrophages and Th cells, we use the parameter values described in Table A.1. We assume that antigen is discovered at time t=0 by the M1 macrophages (which are the primary host defence (Mills and Ley, 2014)). So, the initial values for these simulations are: $M_1(0) = 100$, $M_2(0) = 0$, $H_1(0) = 0$ and $H_2(0) = 0$.

In Fig. 6 we consider the case $a_{H_1}/a_{H_2} = 0.125 \ll 1$, which leads to an

Table A.1
Table summarising the parameters that appear in models (1) and (3), and their values used throughout the numerical simulations. References marked by "*" correspond to parameter values that were approximated based on experimental studies. Some of the elements in column "Value" show not only the specific values used for the simulations, but also the parameter ranges (in parentheses) over which we varied those parameters.

Param.	Description	Value	Units	Ref
α	tumour growth rate	0.69 – 0.97	1/day	*Danciu et al. (2013)
β	carrying capacity of the tumour	10^9	cell	Eftimie et al. (2010),de Pillis et al. (2005)
f	tumour natural death rate	10^{-8}	1/day	Estimate
g_{H_1}	killing rate of tumour cells by the Th1 cells	5×10^{-9}-10^{-7}	1/day	Estimate
g_{H_2}	killing rate of tumour cells by the Th2 cells	10^{-9} (10^{-9} – 10^{-7})	1/day	Estimate
g_{M_1}	killing rate of tumour cells by M1 macrophages	6×10^{-9}	1/((cell)(day))	Estimate
g_{M_2}	tumour growth rate in the presence of M2 cells	2.3×10^{-10}, 7.3×10^{-10} (10^{-10} – 7.3×10^{-9})	1/((cell)(day))	Estimate
n_{H_1}	inactivation rate of Th1 cells by tumour cells	10^{-7}	1/((cell)(day))	Eftimie et al. (2010)
n_{H_2}	inactivation rate of Th2 cells by tumour cells	10^{-7}	1/((cell)(day))	Eftimie et al. (2010)
n_{M_1}	inactivation rate of M1 cells by tumour cells	10^{-7} (10^{-7} – 7×10^{-4})	1/((cell)(day))	Estimate
n_{M_2}	recruitment rate of M2 cells in the presence of tumour cells	10^{-7} (10^{-10} – 10^{-7})	1/((cell)(day))	Estimate
a_{H_1}	activation rate of Th1 cells	0.001–0.008	1/day	Estimate
a_{H_2}	activation rate of Th2 cells	0.001–0.008	1/day	Estimate
a_{M_1}	activation rate of M1 cells	0.001 (10^{-4} – 10^{-2})	1/day	Estimate
a_{M_2}	activation rate of M2 cells	0.001 (10^{-4} – 10^{-2})	1/day	Estimate
m_1	carrying capacity of Th cells	10^8	1/cell	Eftimie et al. (2010)
m_2	carrying capacity of macrophages	10^9	1/cell	* Lee et al. (1985)
p_{H_1}	interaction rate between Th1 cells and type–1 cytokines produced by the M1 cells, which leads to the proliferation of Th1 cells	0.09 (0.009 – 0.17)	1/(day)(cell)	Estimate
p_{H_2}	interaction rate between Th2 cells and type–2 cytokines produced by the M2 cells, which leads to the proliferation of Th2 cells	0.09 (0.009 – 0.17)	1/(day)(cell)	Estimate
p_{M_1}	proliferation rate of M1 cells	0.02 (10^{-3}, 10^{-1})	1/day	Estimate
p_{M_2}	interaction rate between M2 cells and the IL–4 cytokines produced by Th2 cells, which leads to M2 proliferation	0.02	1/(day)(cell)	* Jenkins et al. (2011)
r_{M_1}	M1 → M2 transition rate	0.05–0.09	1/day	Wang et al. (2012)
r_{M_2}	M2 → M1 transition rate	0.05–0.08	1/ day	Wang et al. (2012)
e_{H_1}	death rate of the Th1 cells	0.03	1/day	Magombedze et al. (2014)
e_{H_2}	death rate of the Th2 cells	0.03	1/day	Magombedze et al. (2014)
e_{M_1}	death rate of the M1 cells	0.02	1/day	Magombedze et al. (2014)
e_{M_2}	death rate of the M2 cells	0.02	1/day	Magombedze et al. (2014)

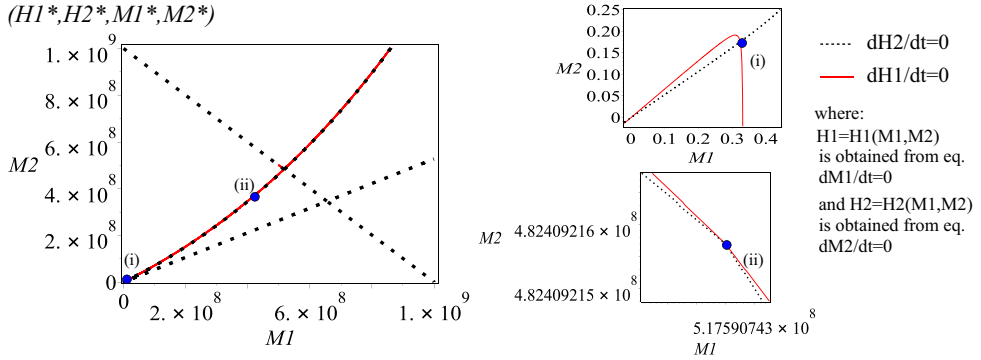

Fig. 4. Steady states (H_1^*, H_2^*, M_1^*, M_2^*) for system (1), as shown by the filled circles marking the intersection of nullclines $dH_1/dt = 0$ and $dH_2/dt = 0$. We emphasise that to graph these curves, we first solved $dM_1/dt = dM_2/dt = 0$ for H_1 and H_2 as functions of M_1 and M_2, and then substituted the expressions for $H_1(M_1, M_2)$ and $H_2(M_1, M_2)$ into the equations for $dH_1/dt = 0$ and $dH_2/dt = 0$. Despite the apparent overlap between the continuous curve for $dH_1/dt = 0$ and the dotted curve for $dH_2/dt = 0$, there are actually only two intersection points (see figures on the right): (i) $M_1^* = 0.324$, $M_2^* \approx 0.175$, $H_1^* = 3.059$, $H_2^* = 0.098$, and (ii) $M_1^* = 5.176 \times 10^8$, $M_2^* \approx 4.824 \times 10^8$, $H_1^* = 5.066 \times 10^7$, $H_2^* = 4.934 \times 10^7$.

immune response characterised by $H_1^* < H_2^*$ (since the activation and growth of H_1 and H_2 cells depends on the magnitudes of a_{H_1} and a_{H_2}; see also equations (1a) and (1b)). Fig. 6(a) illustrates the dynamics of model (1), when we consider $r_{M_1}/r_{M_2} = 1.8 > 1$ and thus $M_1^* > M_2^*$ (a mixed type-I/type-II immune response, as predicted by the bifurcation diagram in Fig. 5(a)). In regard to the transient immune dynamics: during the first 19 days the Th2 response is lower than the Th1 response, but after day 19 the Th1 response becomes lower than the

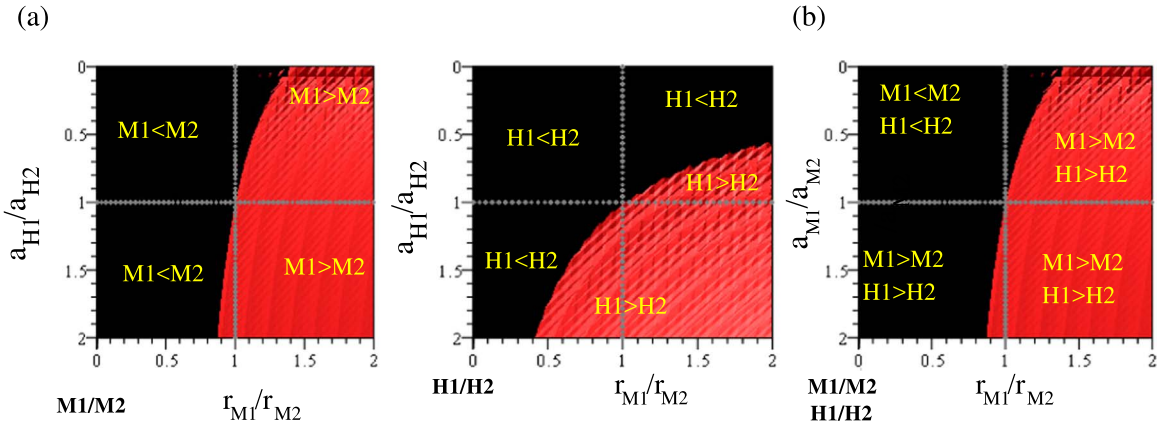

Fig. 5. Bifurcation diagram for the ratio of M_1^*/M_2^* and H_1^*/H_2^* steady states (given by Eqs. (2)), as we change the ratio of: (a) r_{M_1}/r_{M_2} versus a_{H_1}/a_{H_2}; (b) r_{M_1}/r_{M_2} versus a_{M_1}/a_{M_2}. The black surface describes the parameter region where $M_1^*/M_2^* < 1$ or $H_1^*/H_2^* < 1$, while the red surface (gray on black/white print) describes the parameter region where $M_1^*/M_2^* > 1$ or $H_1^*/H_2^* > 1$. Note that for panel (b), the surfaces for H_1^*/H_2^* and M_1^*/M_2^* coincide. A type-I immune response occurs when the red (gray on black/white print) surfaces overlap in each of the panels in (a) and (b). A type-II immune response occurs when the black surfaces overlap in each of the panels (a) and (b). (For interpretation of the references to color in this figure legend, the reader is referred to the web version of this article.)

Th2 response. The large initial Th1 response leads to a large M1 response. Nevertheless, on day 5, the M2 response becomes larger than the M1 response. Around day 25, there is a second switch between the magnitudes of the M1 and M2 responses. Fig. 6(b) illustrates the long-term dynamics of macrophages and Th cells for $r_{M_1}/r_{M_2} = 0.625 < 1$. In this case, the level of M2 macrophages stays higher than the level of M1 macrophages even during transient times (see panel (b)(i) for $t \in (5, 30)$; compare this with panel (a)(i) where $M_1 > M_2$ for $t > 25$). Asymptotically, the solution approaches a steady state with $H_1^* < H_2^*$ and $M_1^* < M_2^*$ (a type-II immune response, as predicted by the bifurcation diagram in Fig. 5(a)).

In Fig. 7 we consider the case $a_{H_1}/a_{H_2} \gg 1$, which leads to an immune response characterised by $H_1^* > H_2^*$. Fig. 7(a) illustrates the dynamics of model (1), when $r_{M_1}/r_{M_2} = 1.8 > 1$ and the long-term dynamics is dominated by a type-I immune response (as predicted by the bifurcation diagram in Fig. 5(a)). In regard to the transient dynamics, as before we observe a double switch in the magnitude of macrophages response. Fig. 7(b) illustrates the dynamics of model (1) for $r_{M_1}/r_{M_2} = 0.625 < 1$. The solution approaches a steady state with $H_1^* > H_2^*$ and $M_1^* < M_2^*$ (i.e., a mixed type-I/type-II immune response,

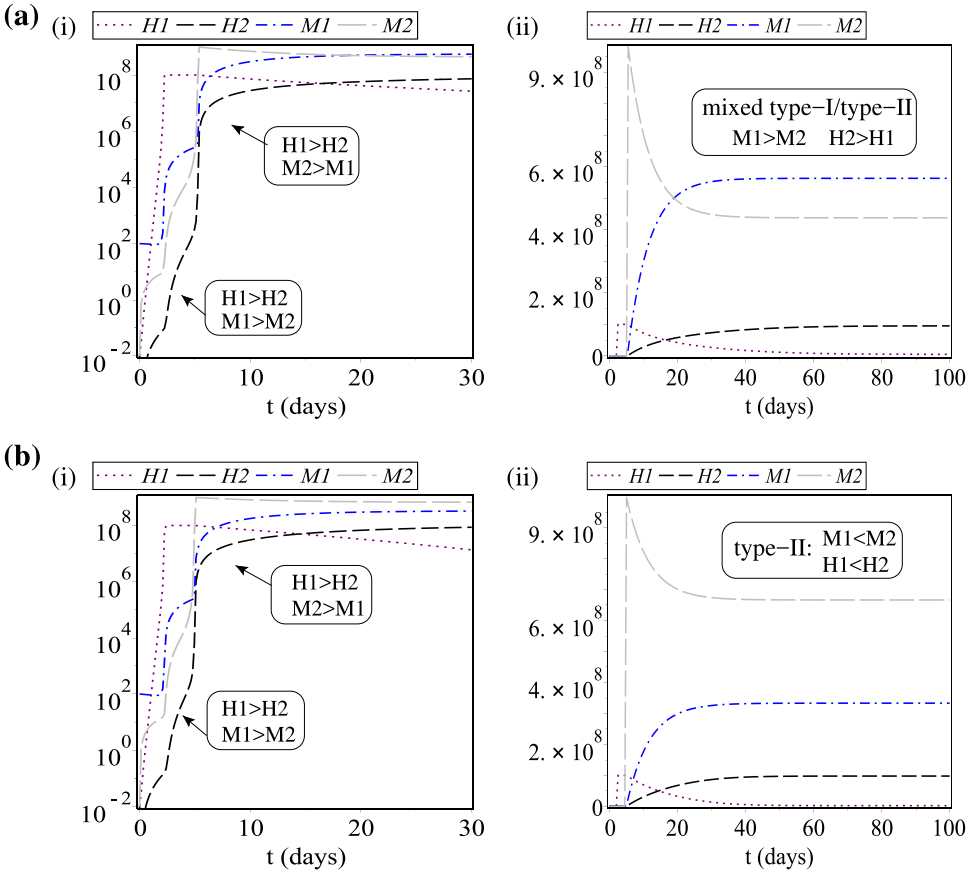

Fig. 6. Dynamics of model (1) for $a_{H_1} = 0.001 < a_{H_2} = 0.008$ (which leads to $H_1^* < H_2^*$). (a) Short-term dynamics (panel (i)) and long-term dynamics (panel (ii)) obtained when $r_{M_1} = 0.09$, $r_{M_2} = 0.05$. b) Short-term dynamics (panel (i)) and long-term dynamics (panel (ii)) when $r_{M_1} = 0.05$, $r_{M_2} = 0.08$. For the rest of parameter values see Table A.1.

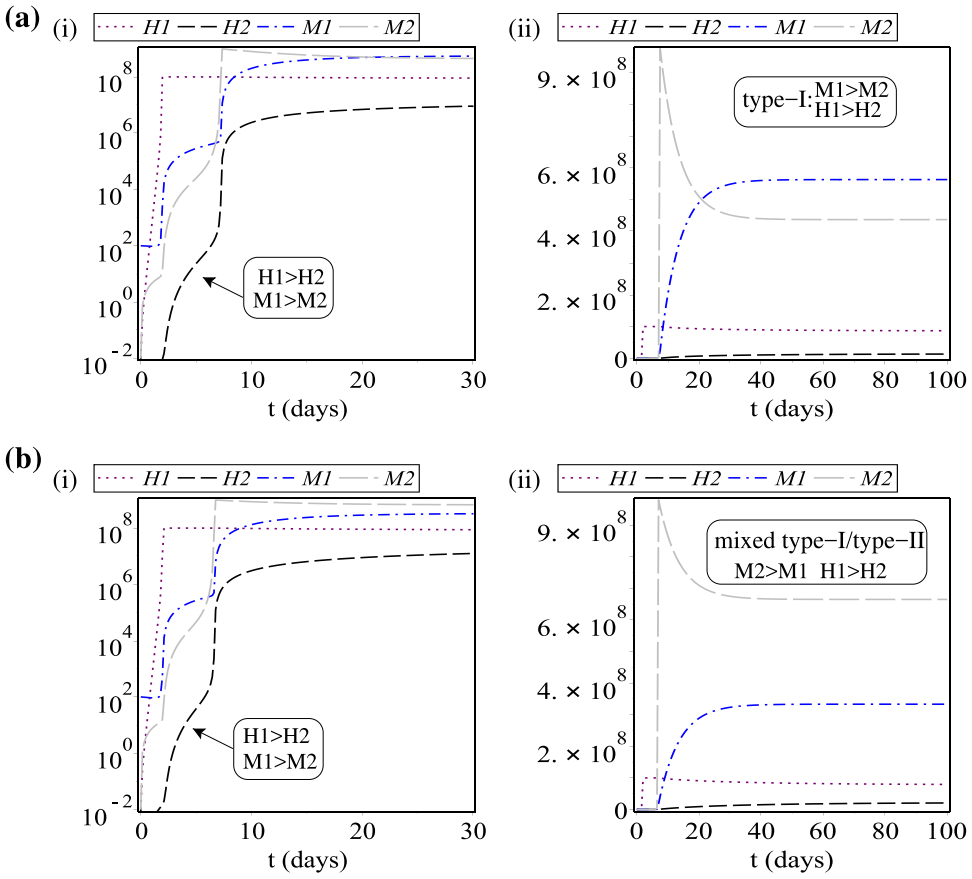

Fig. 7. Dynamics of model (1) for $a_{H_1} = 0.008 > a_{H_2} = 0.001$ (which leads to $H_1^* > H_2^*$). (a) Short-term dynamics (panel (i)) and long-term dynamics (panel (ii)) obtained when $r_{M_1} = 0.09$, $r_{M_2} = 0.05$; b) Short-term dynamics (panel (i)) and long-term dynamics (panel (ii)) obtained when $r_{M_1} = 0.05$, $r_{M_2} = 0.08$. For the rest of parameter values see Table A.1.

as predicted by the bifurcation diagram in Fig. 5(a)).

Note in Figs. 6 and 7 that there are points where the curves have non-continuous derivatives. This is likely a numerical artefact, the result of the number of points used to plot the curves and the scale of the plot.

We conclude that the dynamics of model (1) can be dominated by a type-I, a type-II or a mixed type-I/type-II immune responses, depending on the ratio r_{M1}/r_{M2} and the activation rate of immune cells. Note that for these simulations, we also varied the macrophages activation rates (a_{M_1}, a_{M_2}) within the interval $(10^{-4}, 10^{-2})$, but the overall dynamics did not change. We acknowledge that model dynamics might change if we would vary some of the fixed parameters (i.e., those parameters for which we found values in the literature; see Table A.1).

3. Modelling the Th1 & Th2 and M1 & M2 interactions with tumour cells

Next, we investigate the anti-tumour and pro-tumour effects of M1/M2 macrophages and Th1/Th2 cells. Thus, we consider five variables: the density of tumour cells (T), the density of Th1 cells (H_1), the density of Th2 cells (H_2), the density of M1 macrophages (M_1) and the density of M2 macrophages (M_2). The time-evolution of these variables is given by

$$\frac{dT}{dt} = \alpha T\left(1 - \frac{T}{\beta}\right) - fT - g_{H_1}H_1T - g_{H_2}H_2T - g_{M_1}M_1T + g_{M_2}M_2T, \tag{3a}$$

$$\frac{dH_1}{dt} = a_{H_1}M_1 + p_{H_1}H_1M_1\left(1 - \frac{H_1 + H_2}{m_1}\right) - n_{H_1}H_1T - e_{H_1}H_1, \tag{3b}$$

$$\frac{dH_2}{dt} = a_{H_2}M_2 + p_{H_2}H_2M_2\left(1 - \frac{H_1 + H_2}{m_1}\right) - n_{H_2}H_2T - e_{H_2}H_2, \tag{3c}$$

$$\frac{dM_1}{dt} = a_{M_1}H_1 + p_{M_1}M_1\left(1 - \frac{M_1 + M_2}{m_2}\right) - n_{M_1}M_1T - e_{M_1}M_1 + r_{M_1}M_2 - r_{M_2}M_1, \tag{3d}$$

$$\frac{dM_2}{dt} = a_{M_2}H_2 + p_{M_2}M_2H_2\left(1 - \frac{M_1 + M_2}{m_2}\right) + n_{M_2}M_2T - e_{M_2}M_2 - r_{M_1}M_2 + r_{M_2}M_1. \tag{3e}$$

In addition to the assumptions incorporated in model (1), for model (3) we make also the following assumptions:

- Tumour cells grow at a rate α, up to a carrying capacity β (which is chosen to correspond to the maximum tumour size allowed for experimental protocols in mice (NIH, 1996)). To model the phenomenological observation that tumour growth slows down as tumour becomes very large and depletes the available nutrients (Laird, 1964), we choose logistic growth. Tumour cells have a very low natural death (i.e., apoptosis) rate f (Wong, 2011). The Th1 cells kill the cancer cells at a rate g_{H_1} (via IL −2 and IFN −γ); see Knutson and Disis (2005). Moreover, the tumour cells can be killed by the Th2 cells at a rate g_{H_2} (via IL −4 & IL −13 cytokines that attract eosinophils (Mattes et al., 2003)). Also, M1 macrophages kill tumour cells at a rate g_{M_1} (through the release of tumouricidal products such as NO (Zhang et al., 2014; Lamagna et al., 2006). Finally, the presence of M2 macrophages increases the proliferation of cancer cells (Sica et al., 2008). We denote by g_{M_2} the proliferation rate of cancer cells in the presence of M2 cells. For simplicity, we

assumed that all immune cells interact with tumour cells in a linear manner. Under this assumption, the term modelling tumour proliferation can be written as $T(\alpha + g_{M_2}M_2 - \alpha T/\beta)$, suggesting that the presence of M_2 cells can increase the maximum tumour size. This seems to be confirmed by experimental studies showing that tumours co-inoculated with M2 macrophages grow much larger than control tumours (see, for example, Fig. 5 in Yamaguchi et al. (2016)).

- The Th1 cells can be inactivated by the tumour cells at a rate n_{H_1} (Magombedze et al., 2014; Eftimie et al., 2010). All other rates that control the dynamics of Th1 cells are as described in Section 2.
- The Th2 cells can be inactivated by the tumour cells at a rate n_{H_2} (Magombedze et al., 2014). All other rates that control the dynamics of Th2 cells are as described in Section 2.
- The anti-tumour M1 cell population can be reduced, at a rate n_{M_1}, by the tumour cells that secrete pro-tumour cytokines (e.g., IL −10, TGF-β) (Mantovani et al., 2008). All other rates that control the dynamics of M1 macrophages are as described in Section 2.
- The recruitment of M2 cells at the tumour site is helped by cytokines (e.g., IL −10) and chemokines (e.g., CCL2) produced by the tumour cells (Solinas et al., 2009). We denote this recruitment rate by n_{M_2}. For simplicity, throughout this study we consider $n_{M_2} = n_{M_1}$. All other rates that control the dynamics of M2 macrophages are as described in Section 2.

We emphasise that in model (3), we incorporated only an example of tumour-macrophage-Th cell interactions. Continuous development of this research area, will likely reveal more types of interactions among these cells. However, it is not the goal of this article to model detailed dynamics of tumour-immune interactions. Rather, we plan to investigate whether the assumptions incorporated in (3) can explain the paradoxical anti-tumour and pro-tumour immune dynamics observed experimentally in B16 melanoma cells (as discussed in Section 1).

We also note that while there are many other types of tumour growth laws (e.g., exponential, power, von Bertalanffy, Gompertz or sub-linear) that can fit various experimental data sets, recent studies suggest that the most appropriate growth laws seem to be dependent on the details of the experiments and on the particular tumour cell lines (Murphy et al., 2016; Sarapata and de Pillis, 2014; Benzekry et al., 2014; Talkington and Durrett, 2015). Since the goal of this study is not to compare in detail our results to various experimental data sets, we decided to focus only on one law, the logistic growth, and to investigate whether this assumption on tumour growth can help propose some generic biological mechanisms that can explain the apparent paradox in the observed anti-tumour immune responses.

Before investigating the dynamics of system (3), we note that (3) has non-negative solutions (see the discussion in Appendix B).

3.1. Steady states and stability

Next, we study the long-term behaviour of model (3), when the system is at equilibrium. The existence of four possible equilibrium points (listed below) emphasises the complexity of (3).

1. No tumour cells and no immune cells: $(T^*, H_1^*, H_2^*, M_1^*, M_2^*) = (0, 0, 0, 0, 0)$.
2. No immune cells, but tumour cells present: $(T^*, H_1^*, H_2^*, M_1^*, M_2^*) = (T^*, 0, 0, 0, 0)$, with $T^* = \beta(1 - f/\alpha)$.
3. No tumour cells and all immune cells present: $(T^*, H_1^*, H_2^*, M_1^*, M_2^*) = (0, H_1^*, H_2^*, M_1^*, M_2^*)$ where H_1^*, H_2^*, M_1^* and M_2^* are described in Section 2.1. As before, there are two such states.
4. Presence of all immune and tumour cells: $(T^*, H_1^*, H_2^*, M_1^*, M_2^*)$, where T^*, H_1^*, H_2^*, M_1^* and M_2^* are given implicitly by the following equations:

$$T^* = \beta\left(1 - \frac{g_{H_1}H_1^* + g_{H_2}H_2^* + g_{M_1}M_1^* - g_{M_2}M_2^* + f}{\alpha}\right), \tag{4a}$$

$$M_1^* = \frac{n_{H_1}H_1^*T^* + e_{H_1}H_1^*}{a_{H_1} + p_{H_1}H_1^*\left(1 - \frac{H_1^* + H_2^*}{m1}\right)}, \tag{4b}$$

$$H_1^* = \frac{n_{M_1}M_1^* + e_{M_1}M_1^* + r_{M_2}M_1^* - r_{M_1}M_2^* - p_{M_1}M_1^*(1 - \frac{M_2^* + M_1^*}{m_2})}{a_{M_1}}, \tag{4c}$$

$$M_2^* = \frac{n_{H_2}H_2^*T^* + e_{H_2}H_2^*}{a_{H_2} + p_{H_2}H_2^*\left(1 - \frac{H_1^* + H_2^*}{m1}\right)}, \tag{4d}$$

$$H_2^* = \frac{e_{M_2}M_2^* + r_{M_1}M_2^* - r_{M_2}M_1^* - n_{M_2}M_2^*}{a_{M_2} + p_{M_2}M_2^*(1 - \frac{M_2^* + M_1^*}{m_2})}. \tag{4e}$$

For the parameter values shown in Table A.1, there are three such steady states that are real and positive (see Fig. E.18 in Appendix E), and their stability is illustrated in Fig. E.19(e)–(g).

As in Section 2.1, we are now interested in investigating the parameter space where tumour growth and elimination occurs in the presence of a type-I immune response, a type-II response or a mixed response. Thus, we focus on the two steady states with non-zero immune responses. Since the steady state $(0, H_1^*, H_2^*, M_1^*, M_2^*)$ is similar to the state investigated in Fig. 5, we can conclude that tumour elimination can occur in the presence of a type-I response, a type-II response, or a mixed type-I/type-II response. We will return to this aspect in Section 3.2, when we will investigate numerically the long-term dynamics of system (3).

For the tumour-immune coexistence state $(T^*, H_1^*, H_2^*, M_1^*, M_2^*)$, let us first investigate the parameter values for which $T^* > 0$, which is equivalent (from (4a)) with solving the following equation for $T^* > 0$:

$$\alpha - T^*\frac{\alpha}{\beta} - f - g_{H_1}H_1^* - g_{H_2}H_2^* - g_{M_1}M_1^* + g_{M_2}M_2^* = 0. \tag{5}$$

Note in Eqs. (4c)–(4e) that $H_{1,2}^*$ can be expressed in terms of $M_{1,2}^*$. In addition, we can make the assumption that $M_1^* + M_2^* \approx m_2$ (assumption supported by the numerical results; see Figs. 10–12). This allows us to re-write the condition for the existence of the state $T^* > 0$ as

$$\frac{\alpha}{\beta}T^* = \alpha - f - \frac{g_{H_1}a_{H_1m_2}(M)}{(n_{H_1}T + e_{H_1})(1 + M)} - \frac{g_{H_2}a_{H_2}m_2}{(n_{H_2}T^* + e_{H_2})(1 + M)} - g_{M_1}\left(m_2 - \frac{m_2}{1 + M}\right) + \frac{g_{M_2}m_2}{1 + M}, \tag{6}$$

where $M = M_1^*/M_2^*$. We graph this equation in Figs. 8 (for lower g_{M_1}: $g_{M_1} = 6 \times 10^{-9}$) and Fig. 9 (for higher g_{M1}: $g_{M_1} = 6 \times 10^{-8}$), to study the changes in the parameter space where $T^* > 0$, as we vary g_{M_2}, g_{H_1} and g_{H_2}.

In Fig. 8, we notice that for low g_{M_2} values (see panels (a), (a'); where $g_{M_2} = 2.3 \times 10^{-10}$), the existence of a tumour-immune coexistence state requires $M = M_1^*/M_2^* \ll 1$ and $H = H_1^*/H_2^* \ll 1$, which is equivalent to a type-II immune response. Increasing g_{M_2} (see panels (b), (b'); where g_{M_2} is increased 30 times, to $g_{M_2} = 6.9 \times 10^{-9}$) can

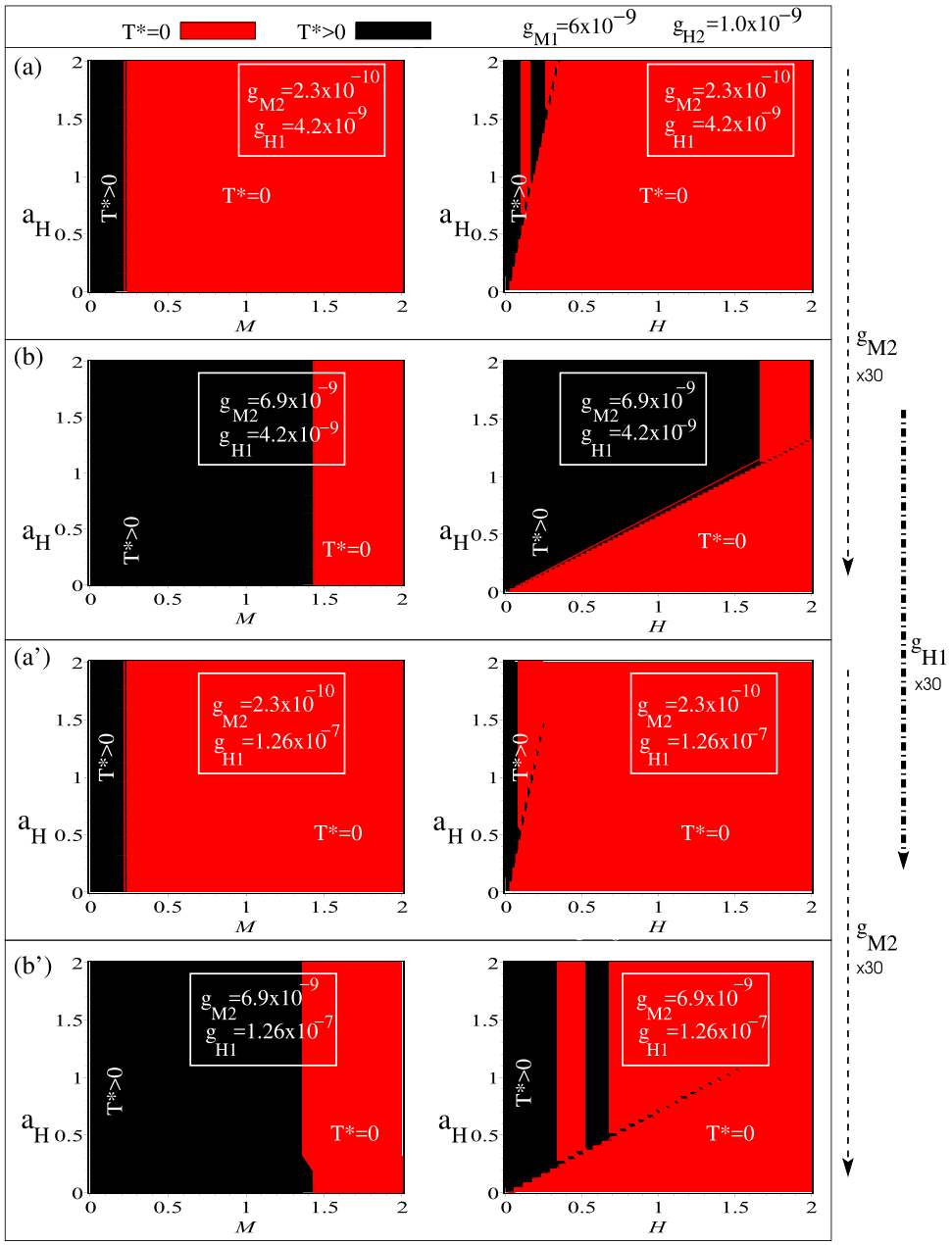

Fig. 8. Parameter space where a tumour-immune coexistence steady state with $T^* > 0$ can exist. Here we show tumour size T^* vs. a_H vs. $M = M_1^*/M_2^*$ or $H = H_1^*/H_2^*$, as we vary g_{M_2} (increased 30-fold from 2.3×10^{-10} to 6.9×10^{-9}) and g_{H1} (increased 30-fold from 4.2×10^{-9} to 1.26×10^{-7}): (a) $g_{M_2} = 2.3 \times 10^{-10}$, $g_{H_1} = 4.2 \times 10^{-9}$; (b) $g_{M_2} = 6.9 \times 10^{-9}$, $g_{H_1} = 4.2 \times 10^{-9}$; (a') $g_{M_2} = 2.3 \times 10^{-10}$, $g_{H_1} = 4.2 \times 30 \times 10^{-9} = 1.26 \times 10^{-7}$; (b') $g_{M_2} = 6.9 \times 10^{-9}$, $g_{H_1} = 4.2 \times 30 \times 10^{-9} = 1.26 \times 10^{-7}$. Here we chose $g_{H_2} = 1 \times 10^{-9}$, $g_{M_1} = 6 \times 10^{-9}$, $a_{H_2} = 0.001$ and vary a_{H_1} in the ratio $a_H = a_{H_1}/a_{H_2}$. The rest of parameter values are as in Table A.1.

increase the values of the ratio M_1^*/M_2^* for which $T^* > 0$ can exist. These results suggest that, for the g_{M_2} values investigated in this study (panels (a), (a')), whenever tumours grow they are accompanied by a type-II immune response. However, for very large g_{M_2} values, tumours can exist also for $M > 1$ and $H > 1$ (see panels (b), (b')). This result suggests that there could be fewer M2 cells compared to M1 cells, but if these cells secrete large amounts of type-II cytokines, they can skew the tumour microenvironment in favour of tumour sustenance and growth. (We will return to this hypothesis in the Discussion section.) We also need to emphasise here that an increase in g_{H_1} (from 4.2×10^{-9} in panels (a), (b), to 1.26×10^{-7} in panels (a'), (b')) reduces the parameter space over which we can expect tumour-growth in the presence of a type-I response.

In Fig. 9 we notice that the 10-fold increase in g_{M_1} (from $g_{M_1} = 6 \times 10^{-9}$ in Fig. 8 to $g_{M_1} = 6 \times 10^{-8}$ here) has two main effects: (i) forces $T^* > 0$ to exist mainly during a type-II response, and (ii) induces the requirement for much higher g_{M_2} values for tumour persistence in the presence of a type-I response (i.e., at least a 150-fold increase in g_{M_2}; see panels (b), (b'), where only a mixed type-I/type-II response was obtained after a 126-fold increase in g_{M_2}). We emphasise here that small changes in g_{H_2} do not have a significant effect on tumour growth (also supported by the sensitivity analysis in Fig. 14). To observe a difference between the diagrams in panels (a), (b) and those in panels (a'), (b') we had to increase g_{H_2} by more than 40-fold (shown in panels (a'), (b') is the effect of a 60-fold increase in g_{H_2}). In this case, the increase in g_{H_2} affected mainly the region where

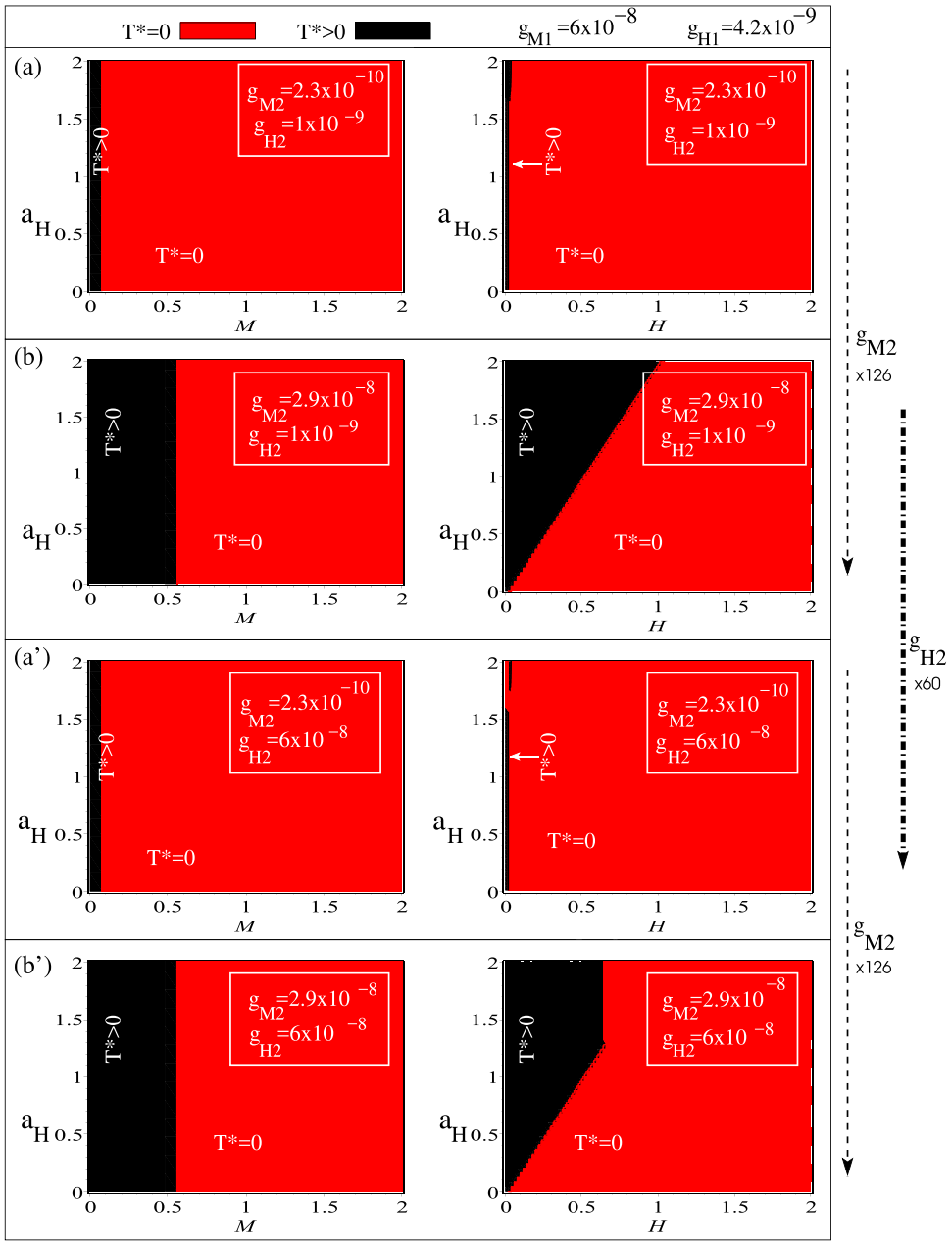

Fig. 9. Parameter space where a tumour-immune coexistence steady state with $T^* > 0$ can exist. Here we show tumour size T^* vs. a_H vs. $M = M_1^*/M_2^*$ or $H = H_1^*/H_2^*$, for $g_{M_1} = 6 \times 10^{-8}$ and different parameter values for g_{M_2} (increased 126-fold from 2.3×10^{-10} to 2.9×10^{-8}) and g_{H_2} (increased 60-fold from 1×10^{-9} to 6×10^{-8}): (a) $g_{M_2} = 2.3 \times 10^{-10}$, $g_{H_2} = 10^{-9}$; (b) $g_{M_2} = 2.9 \times 10^{-8}$, $g_{H_2} = 10^{-9}$; (a') $g_{M_2} = 2.3 \times 10^{-10}$, $g_{H_2} = 6 \times 10^{-8}$; (b') $g_{M_2} = 6.9 \times 10^{-9}$, $g_{H_2} = 6 \times 10^{-8}$. Here we chose $g_{H_1} = 4.2 \times 10^{-9}$, $a_{H_2} = 0.001$ and vary a_{H_1} in the ratio $a_H = a_{H_1}/a_{H_2}$. The rest of parameter values are as in Table A.1.

$H = H_1^*/H_2^* > 1$ (see the right figures in panels (b), (b')).

Overall, Figs. 8 and 9 suggest that the parameters most likely to impact tumour growth/decay are g_{H_1}, g_{M_2} and g_{M_1}. We will return to this aspect in Section 3.3, when we will perform a sensitivity analysis for the transient dynamics of model (3).

3.2. Short-term and long-term dynamics

To investigate numerically the long-term dynamics of immune cells and cancer cells, we use the parameter values described in Table A.1. We chose to use the same parameter values as in Section 2.2, to investigate the effect of introducing a tumour on the interactions between Th cells and macrophages. The initial values for our simulations are: $T(0) = 10^5$, $M_1(0) = 100$, $M_2(0) = 0$, $H_1(0) = 0$ and $H_2(0) = 0$. As before, we chose $M_1(0) > 0$ since the M1 macrophages are the primary host defence (Mills and Ley, 2014).

Tumour elimination. First, we focus on the parameter ranges for r_{M1} and r_{M2} that ensure tumour elimination in the presence of a type-I immune response, a type-II immune response, or a combination of both type-I/type-II immune responses. In this case, the dynamics will approach the stable steady state $(0, H_1^*, H_2^*, M_1^*, M_2^*)$, and the dominant immune responses are consistent with those in the bifurcation diagram shown in Fig. 5. We emphasise this aspect by discussing separately the following two cases involving the activation rates a_{H_1}, a_{H_2} for the Th1 and Th2 cells:

(1) *Case* $a_{H_1} < a_{H_2}$. Fig. 10 illustrates the short-term dynamics (panels (i); $t < 30$ days) and long-term dynamics (panels (ii); $t \leq 100$ days)

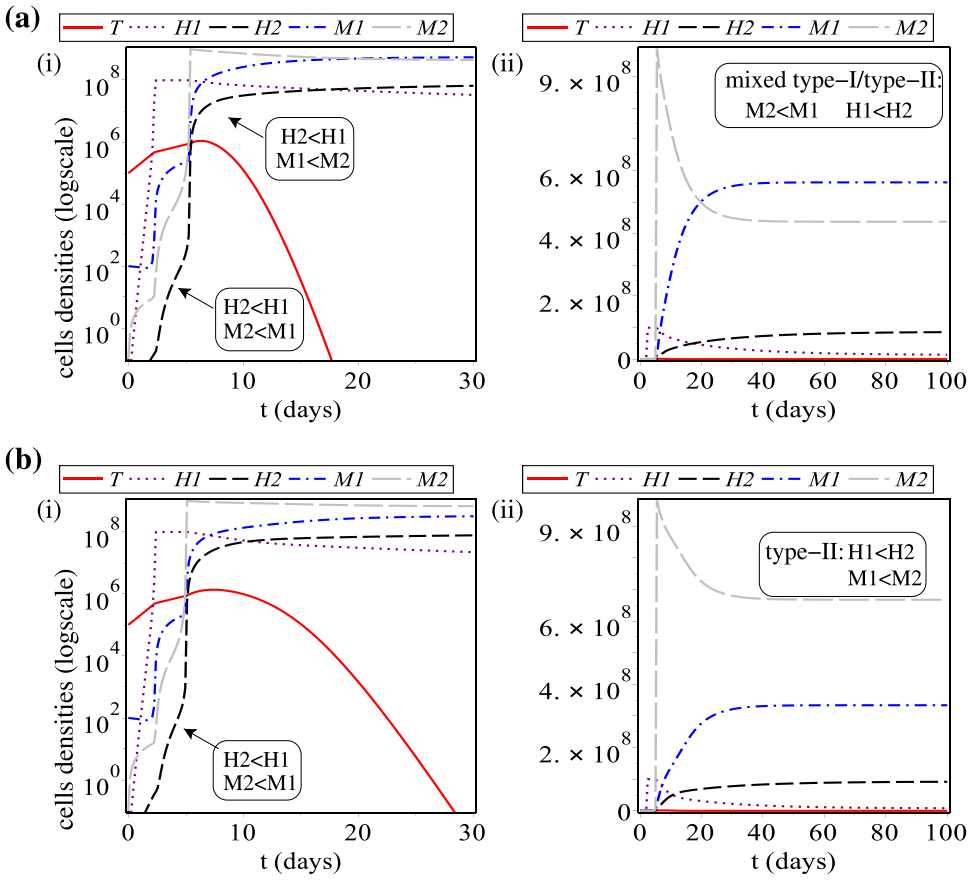

Fig. 10. Dynamics of model (3), when $a_{H_1} = 0.001 < a_{H_2} = 0.008$ and the tumour is eliminated. For this case, we always have $H_1^* < H_2^*$. (a) Short-term dynamics (panel (i)) and long term dynamics (panel (ii)) when $r_{M_1} = 0.09$, $r_{M_2} = 0.05$. (b) Short-term dynamics (panel (i)) and long-term dynamics (panel (ii) for $r_{M_1} = 0.05$, $r_{M_2} = 0.08$. For these simulations we also choose: $g_{H_1} = 4.8 \times 10^{-9}$, $g_{M_2} = 2.3 \times 10^{-10}$, $\alpha = 0.69$. For the rest parameters values see Table A.1.

of model (3), for two different cases: (a) $r_{M_1}/r_{M_2} = 1.8 \gg 1$, and (b) $r_{M_1}/r_{M_2} = 0.625$. In panel (a)(i) we observe a double switch between the M1 and M2 cells that dominate the dynamics (and this is associated with only one switch in the Th1-Th2 dynamics). In panel (b)(i) we observe a single switch the dynamics of both M1 and M2 cells, and Th1 and Th2 cells. In all cases the tumour is eliminated, and the results are consistent with the bifurcation diagrams in Fig. 5(a).

(2) *Case* $a_{H_1} > a_{H_2}$. Fig. 11 illustrates the short-term dynamics (panels (i)) and long-term dynamics (panels (ii)) of model (3) for two cases: (a) $r_{M_1}/r_{M_2} = 1.8$, (b) $r_{M_1}/r_{M_2} = 0.625$. In panel (a)(i) we observe a double switch between the M1 and M2 cells that dominate the dynamics (but this is not associated with any switch in the Th1-Th2 dynamics). In panel (b)(i) we observe a double switch between the Th1 and Th2 cells that dominate the dynamics (associated with a single switch in the M1-M2 dynamics).

Tumour persistence. Fig. 12(a) shows tumour growth for $r_{M_1}/r_{M_2} = 1$ (and $g_{H_1} = 4.2 \times 10^{-9}$, $g_{M_2} = 7.3 \times 10^{-10}$). In the long term, the dynamics of system (3) approaches the stable steady state (T^*, H_1^*, H_2^*, M_1^*, M_2^*). By investigating the short-term dynamics of model (3) (see panel a(i)) we observe a switch in both the Th1-Th2 and M1-M2 dynamics, from an initial type-I response to a later type-II response. This is consistent with the bifurcation results in Fig. 8(b), where tumour exists for $M, H \ll 1$ (where $M = M_1^*/M_2^*$, $H = H_1^*/H_2^*$). Moreover, we would like to emphasise that the dormant behaviour exhibited by the tumour for $t \in (5, 15)$ is mainly the result of a very large M1 population that keeps the tumour under control. As soon as this M1 population is reduced, the tumour grows fast towards its carrying capacity.

The difference between tumour dormancy/growth in Fig. 12 and tumour elimination in Figs. 10 –11 is the result of (a) a small change in the rate at which tumour cells are eliminated by the Th1 cells via the cytokines they produce (from $g_{H_1} = 4.4 \times 10^{-9}$ for tumour elimination to $g_{H_1} = 4.2 \times 10^{-9}$ for tumour growth), and (b) a small change in the rate at which M_2 macrophages can support tumour growth (from $g_{M_2} = 2.3 \times 10^{-10}$ for tumour elimination to $g_{M_2} = 7.3 \times 10^{-10}$ for tumour growth). However, different other combinations of parameter changes can lead to similar tumour dormant behaviours (which seem to be controlled by relatively high levels of M1 cells). To investigate the effect of small changes in parameter values on the level of tumour and immune cells during dormancy (not only M1 but also M2, Th1 and Th2 cells), in Section 3.3 we will perform a sensitivity analysis.

In Section 1 we mentioned the experimental results in Chen et al. (2011) (see also Fig. 2(c)), which showed tumour growth being associated with a shift in the ratio of M1 and M2 cells: from M1:M2 ≈ 90:10 on day 7, to M1:M2 ≈ 20:80 on day 14. To compare these experimental results with our numerical results, in Fig. 12(b) we show the percentage of Th cells and macrophages on day 4.5 (when tumour is small), day 14 (when tumour is dormant) and day 19 (when tumour approaches its carrying capacity). We see that tumour growth is not only associated with an increase in the percentage of M2 cells (as shown experimentally in Chen et al. (2011)), but also with an increase in the percentage of Th2 cells (as shown experimentally in Protti and Monte (2012)). Note that this is one possible outcome of the model. Changes in parameter values could lead to different ratios of Th2:Th1 cells and M2:M1 cells as tumour progresses.

Finally, we recall that the results in Fig. 8(b) suggested that by increasing g_{M_2} one could observe tumour existence also in the case of a

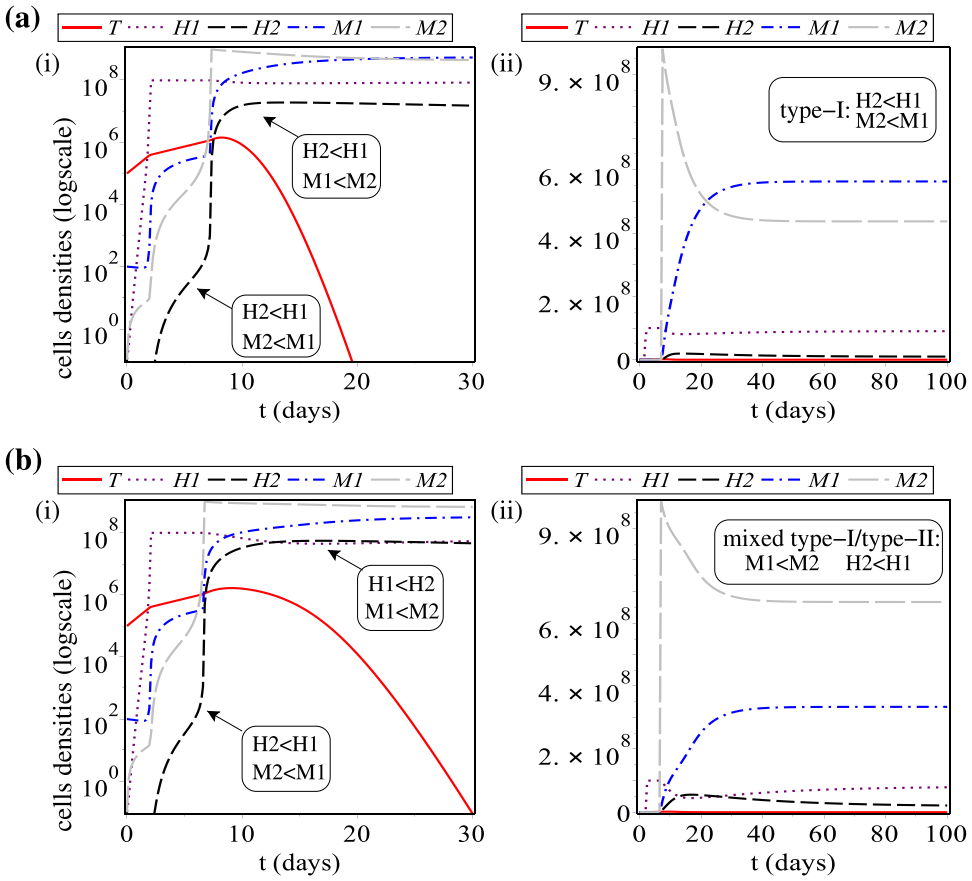

Fig. 11. Dynamics of model (3) when $a_{H_1} = 0.008 > a_{H_2} = 0.001$ and the tumour is eliminated. For this case, we always have $H_1^* > H_2^*$. (a) Short-term dynamics (panel (i)) and long-term dynamics (panel (ii)) for $r_{M_1} = 0.09$, $r_{M_2} = 0.05$. (b) Short-term dynamics (panel (i)) and long-term dynamics (panel (ii)) for $r_{M_1} = 0.05$, $r_{M_2} = 0.08$. For these simulations we also choose $g_{H_1} = 4.8 \times 10^{-9}$, $g_{M_2} = 2.3 \times 10^{-10}$, $\alpha = 0.69$. For the rest of parameters values see Table A.1.

type-I immune response with $M, H > 1$ (in addition to a type-II response, with $M, H < 1$). We show in Fig. 13 the short-term and long-term dynamics of model (3), characterised by the persistence of tumour cells at lower values (with a maximum of about $5{\times}10^7$ cells). This persistence is the result of a type-I immune response, which alternates for short periods of time with a type-II response. We emphasise that these oscillations in tumour growth/decay (triggered by oscillations in the type-I/type-II immune responses) might not be always observable in a clinical setting. Friberg and Mattson (1997) showed that in humans, the tumour diagnostic level is between 10^7 and 10^9 cells. Therefore, $5{\times}10^7$ cells might not be always detected clinically.

3.3. Sensitivity analysis

Since the majority of parameter values could not be approximated from the literature, in the following we perform a sensitivity analysis to investigate the effect of changes in these parameters on the growth of the tumour. To this end, we vary each parameter P by $\pm 10\%$ or $\pm 90\%$ at a time (i.e., $P \pm \triangle P$, with $\triangle P = 0.1P$ or $\triangle P = 0.9P$), and investigate the impact of this change on tumour size on day 10 (an arbitrarily-chosen day, when the tumour has not reached its maximum size yet). The relative change in tumour size on day 10 (i.e., $\triangle T(10)$) is used in Fig. 14 to plot the ratio of relative changes: $(\frac{\triangle T(10)}{T(10)})/(\frac{|\triangle P|}{|P|})$.

Fig. 14 illustrates tumour sensitivity to changes in the parameter values: (a) by $\pm 10\%$ and (b) by $\pm 90\%$. The parameters that have the most significant effect on tumour size when varied by $\pm 10\%$ are: the tumour growth rate (α), the proliferation of Th1 cells (p_{H_1}), the elimination rate of tumour cells by the Th1 cells (g_{H_1}) and by M1 macrophages (g_{M_1}), the carrying capacity of Th cells (m_1), the carrying capacity of macrophages (m_2), the transition rate from M1 to M2 cells (r_{M_1}), the activation rate of M1 cells (a_{M_1}) and the proliferation of M2 cells in the presence of type-II cytokines (p_{M_2}). It is likely that p_{M_1} might also have higher impact on tumour if we would consider higher self-proliferation rates for M1 cells. The parameters that have the most significant impact on tumour size when varied by $\pm 90\%$ are p_{H_1} and α (similar to case (a)). Also a decrease in m_1, g_{H_1}, g_{M_1} and r_{M_1} leads to a significant increases in tumour size (see the inset in the right panel of Fig. 14(b)). (Note that, in Fig. 14(b) is difficult to see the reduction in tumour size as we vary the parameter values – because of the very large increases in tumour size.) We also need to emphasise that g_{H_2} and g_{M_2} (both associated with a type-II immune response) do not have a significant impact on tumour reduction. This is a particularly interesting result that might be of biological interest, since at least g_{H2} has the same order of magnitude – see Table A.1 – as parameters g_{H_1} and g_{M_1} (which have a significant effect on tumour reduction/growth). Moreover, this result supports the idea that the elimination of tumour cells by the Th2 cells in Mattes et al. (2003) was not the result of direct Th2-tumour interactions (via Th2-cytokines), but the combined effect of different anti-tumour cells.

To gain a better understanding on tumour dormancy (and on the role of immune response in controlling tumour growth), next we perform a tumour and immune sensitivity to small changes in four parameter values associated with anti-tumour/pro-tumour immune responses: g_{H_1}, g_{H_2}, g_{M_1}, g_{M_2}. To this end, we start with the baseline parameters that lead to tumour dormancy/growth in Fig. 12(a), and we vary them by $\pm 10\%$ to investigate the changes in tumour and immune sizes at day t=10 (when dormancy occurs). First, we note that during tumour dormancy, changes in parameter g_{H_1} have a slightly bigger

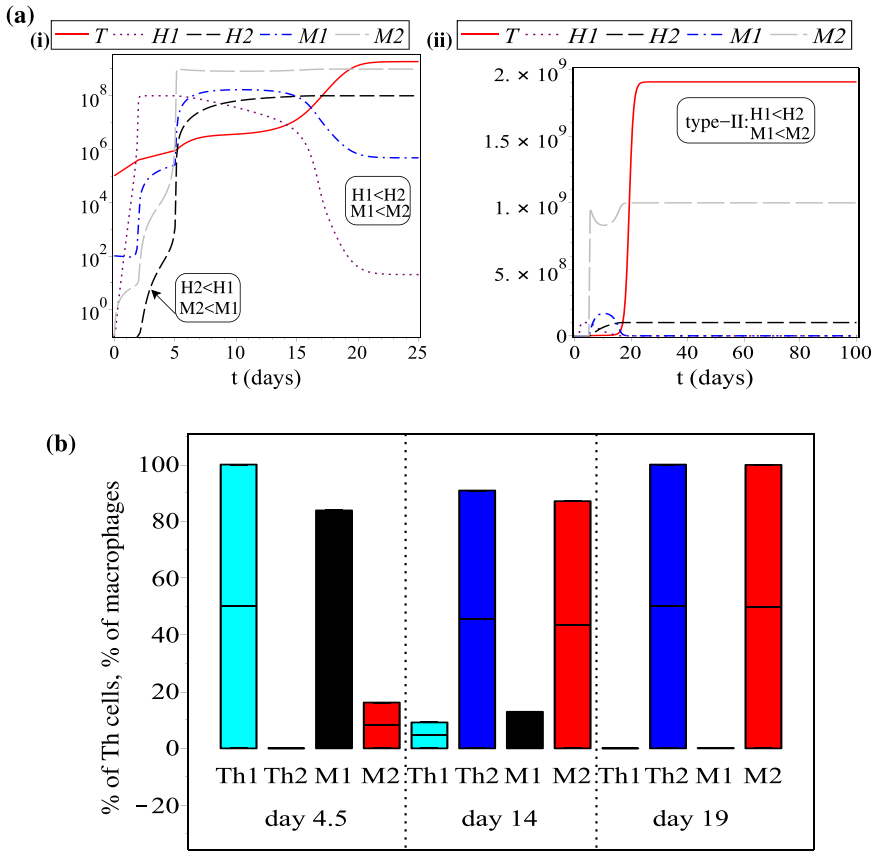

Fig. 12. (a) Tumour growth exhibited by model (3), when $a_{H_1} = a_{H_2} = 0.008$ and $r_{M_1} = 0.09$, $r_{M_2} = 0.05$. Note that tumour growth is associated with a type-II immune response: $M_1^* < M_2^*$ and $H_1^* < H_2^*$. (i) short-term dynamics ($t < 25$; the y-axis is shown on a log-scale); (ii) long-term dynamics. Here we choose: $g_{H_1} = 4.2 \times 10^{-9}$, $g_{M_2} = 7.3 \times 10^{-10}$, $\alpha = 0.69$. For the rest of parameters values see Table A.1. (b) Percentage of Th cells and macrophages calculated on 3 different days (t=4.5, t=14, t=19), for the numerical simulations shown in (a).

impact on tumour at day t=10 ($T(10)$) compared to changes in parameter g_{M_1} - see Fig. 15(a). This is in contrast to the case of tumour elimination (see Fig. 14(a), left panel) where g_{M_1} has a bigger impact on $T(10)$ compared to g_{H_1}. Second, we note that during tumour dormancy g_{M_2} has a stronger impact on $T(10)$ (see Fig. 15(a)) compared to the case of tumour elimination where g_{M_2} barely affects $T(10)$ (see Fig. 14(a)). In fact, we observe that ±10% changes in the three parameters g_{H_1}, g_{M_1} and g_{M_2}, lead to changes of relatively similar magnitudes in tumour cells (Fig. 15(a)), and in each of the four types of immune cells (Figs. 15(b)-(d)). This suggest that tumour dormancy is the result of a delicate balance between the anti-tumour effect of Th1 and M1 cells, and the pro-tumour effect of M2 cells. Moreover, by looking at panels (b)-(e) we observe that the effects of g_{M_1} and g_{M_2} do not balance perfectly during dormancy: g_{M_2} causes slightly larger effects in both tumour and immune responses compared to g_{M_1} (and this imbalance eventually translates into tumour relapse).

To conclude the discussion on the effects of parameters g_{H_1}, g_{M_1} and g_{M_2} on the immune responses during tumour dormancy, we stress that while it was expected that an increase in g_{M_1} and g_{H_1} would be associated with an increase in M_1 and H_1 (through the direct reduction of tumour), it was however unexpected that g_{H_1} would have an effect on H_2 and M_2 cells (stronger than the effects of parameters g_{H_2} and g_{M_2}).

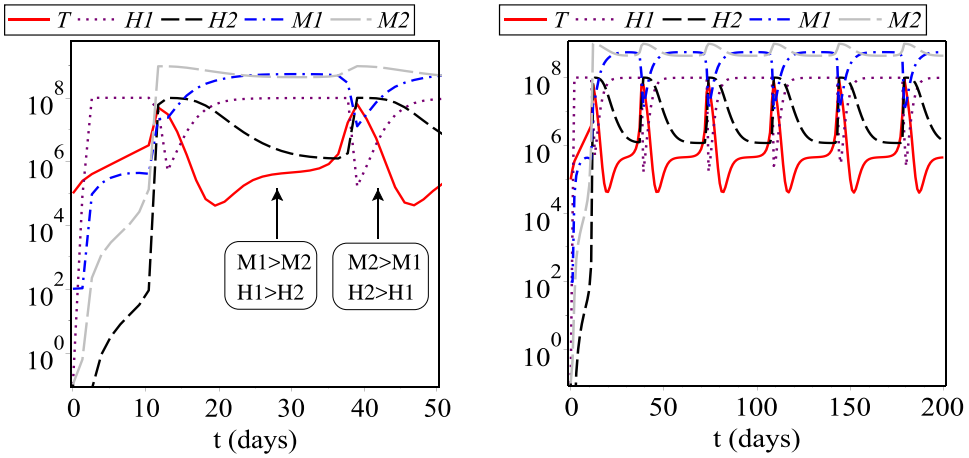

Fig. 13. Short-term dynamics (panel (a)) and long-term dynamics (panel (b)) of model (3), when $g_{M_2} = 7.3 \times 10^{-9}$, $g_{H_2} = 8.546835 \times 10^{-9}$, $a_{H_1} = 0.08 \gg a_{H_2} = 0.001$, $r_1 = 0.09 \gg r_2 = 0.005$. For the rest parameters values see Table A.1. In this case, the tumour persists being controlled alternatively by a type-I and a type-II immune response.

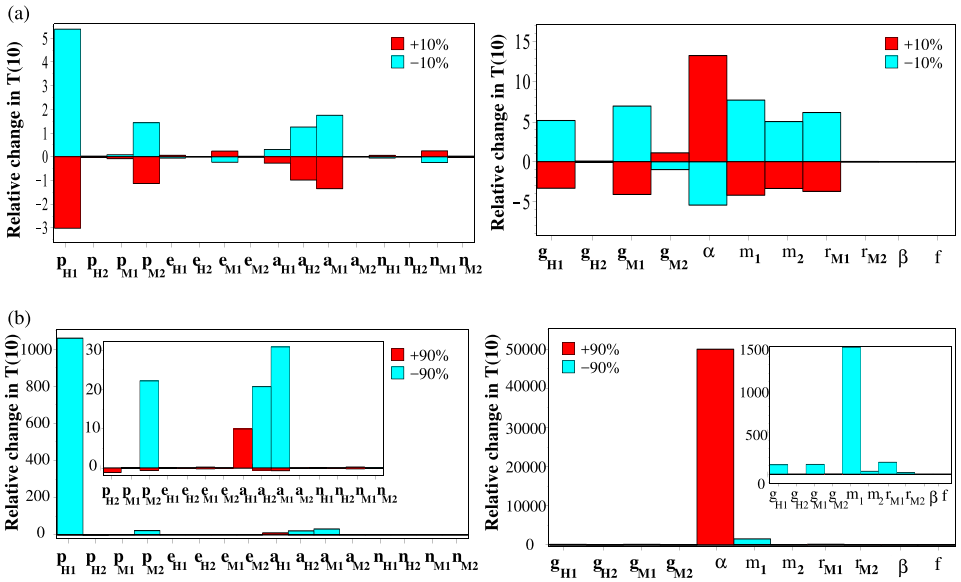

Fig. 14. Sensitivity analysis for model (3), when each model parameter is increased (red bars) and decreased (cyan bars) by: (a) 10% and (b) 90%. Here, we show the relative changes in tumour size on day t=10 in response to the changes in the parameter P values: $(\triangle T(10)/T(10))/(|\triangle P|/|P|)$, with the negative values showing the decrease in tumour size, and the positive values showing the increase in tumour size. The baseline parameters are those shown in Table A.1. The inset figures in panel (b) show the details of the sensitivity analysis for the parameters that do not lead to the two largest changes in tumour size (i.e., after we remove p_{H_1} and α from the bar plots). (For interpretation of the references to color in this figure legend, the reader is referred to the web version of this article.)

4. Summary and discussion

In this article, we derived two mathematical models for the dynamics of immune responses involving Th1 & Th2 and M1 & M2 cells, in the absence and in the presence of tumour cells. We then used these models to propose mechanistic hypotheses that could explain the contradictory results in the experimental data for the immune response against melanoma B16 cells.

We started with a model that considered only the interplay between M1 and M2 macrophages, and Th1 and Th2 cells in response to some external pathogen that first triggered an M1 response (i.e., $M_1(0) > 0$). To shed light on the complexity of model dynamics, we first calculated the steady states (to study the long-term behaviour of the model) and then we performed numerical simulations for the short-term and long-term model dynamics. By focusing on the ratio r_{M_1}/r_{M_2} (of macrophages re-polarisation rates), and the activation rates of Th cells (a_{H1}, a_{H2}) in the presence of signals received from macrophages, we were able to classify the immune responses into: a type-I dominated response ($H_1 > H_2$, $M_1 > M_2$), a type-II dominated response ($H_1 < H_2$, $M_1 < M_2$), or a combination of type-I and type-II responses (e.g., $M_1 > M_2$ but $H_1 < H_2$); see the results in Figs. 6, 7. Note that experimental studies have shown that different diseases associated with the Th1 and Th2 immune responses can show different levels of M1 and M2 macrophages. For example, in Barros et al. (2013) (Table 1), the authors showed that about 60.7% of Th1 disease cases investigated (in the context of infectious mononucleosis and Crohn's disease) have M1>M2, and about 72.5% of Th2 disease cases investigated (in the context of allergic nasal polyps, oxyuriasis, wound healing and foreign body granulomas) have M2 > M1. Thus their results suggest that there are Th1 diseases with a higher level of M2 cells, and Th2 diseases with a higher level of M1 cells (consistent with our numerical results).

Next, we generalised the mathematical model to consider also tumour dynamics. We showed numerically that tumour elimination can occur both in the presence of a type-I dominated immune response, as well as in the presence of a type-II dominated response (as observed experimentally in Mattes et al. (2003), Xie et al. (2010), Kpbayashi et al. (1998); see also Figs. 1 and 2). We need to emphasise that tumour elimination also required a relatively large tumour lysis rates g_{H_1} and g_{M_1} and a low g_{M_2}. As before, the type of immune response that dominated the dynamics was decided by the ratio r_{M_1}/r_{M_2} and the activation level of immune cells (a_{H1}, a_{H2}).

Tumour growth towards carrying capacity (or some very large size) was always associated in our study with a long-term type-II immune response, i.e., $H_2 > H_1$, $M_2 > M_1$; see Fig. 12. In this case, the initial type-I response (with $M_1 > M_2$ for $t \leq 5$ days and $H_1 > H_2$ for $t \leq 10$ days) was always replaced in the long-term by a type-II immune response. This shift from a type-I to a type-II response was observed also experimentally in the context of cancer growth. For example, Chen et al. (2011) showed a 90:10 ratio of M1:M2 macrophages in B16F10 melanoma tumours around day 7, and a 20:80 ratio of M1:M2 macrophages around day 14 (see Fig. 2(c)). Other experimental studies have described a shift from a Th1 response to a Th2 response during the first 14–20 days of progression of malignant tumours (see Tatsumi et al., 2002 for human melanoma). These experimental studies also suggested that one could improve cancer outcome by re-polarising the macrophages and Th cells from a type-II response associated with tumour growth to a type-I response associated with tumour decay (Heusinkveld and van der Burg, 2011). Our theoretical results are in agreement with the experimental suggestion that a type-I response improves long-term cancer outcome. Moreover, our results also emphasise the complexity of the tumour-immune system, in which a type-I immune response might alternate with a type-II immune response (for short-term or long-term), thus leading only to tumour control but not tumour elimination.

We stress that the interaction between the pro-tumour/anti-tumour effects of macrophages and Th cells affects tumour dynamics in a nonlinear manner. For example, a 10-fold increase in the rate of tumour clearance by M1 macrophages (g_{M_1}) caused tumour persistence only in the presence of a type-II immune response (i.e., a type-I immune response would be associated to tumour clearance). To ensure tumour persistence also in the presence of a type-I response, the 10-fold increase in g_{M_1} needed to be counter-balanced by at least a 150-fold increase in the tumour growth rate in the presence of M2 cells, g_{M_2} (see Figs. 8 and 9). This nonlinearity in the anti-tumour response is likely the result of the interplay between the macrophages and the Th cells, an aspect not very well studied at experimental level. Although there

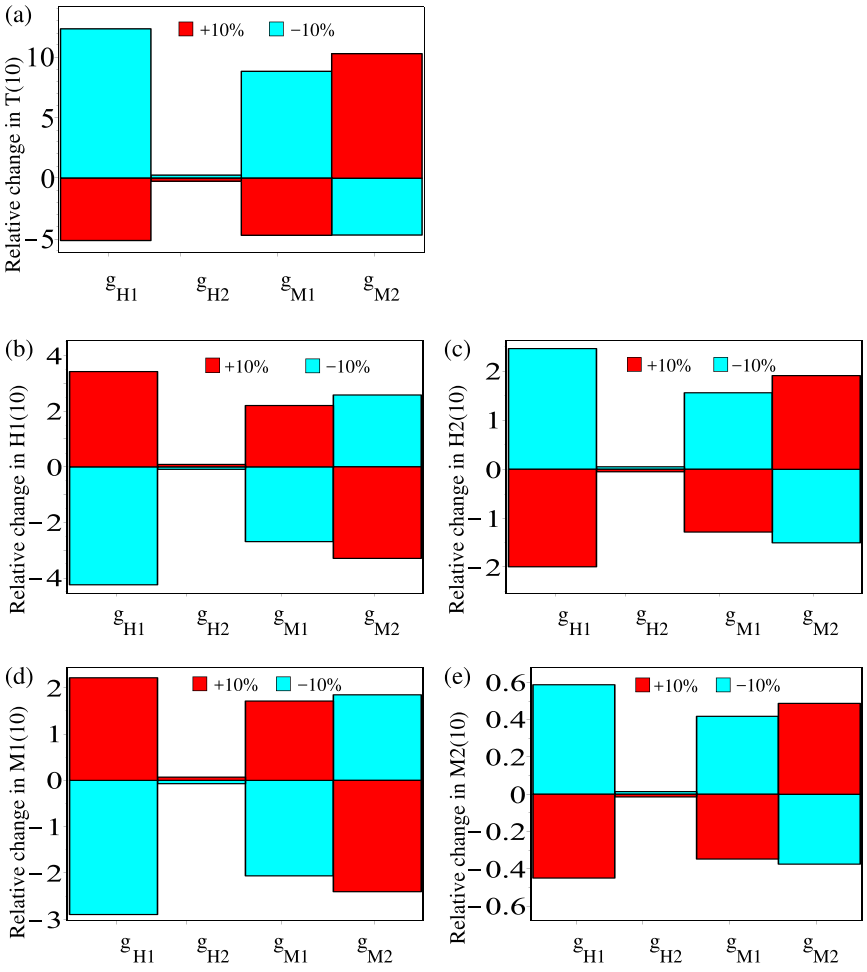

Fig. 15. Sensitivity analysis of the tumour and immune responses for model (3), during tumour dormancy. We focus on four model parameters (g_{H_1}, g_{H_2}, g_{M_1}, g_{M_2}), and increase them (red bars) and decrease them (cyan bars) by 10%. We also show the relative changes in tumour size and all four immune cells on day t=10 in response to the changes in the parameter P values: $(\triangle M_i(10)/M_i(10))/(|\triangle P|/|P|)$ and $(\triangle H_i(10)/H_i(10))/(|\triangle P|/|P|)$, for i=1,2: (a) Relative change in $T(10)$; (b) Relative change in $H_1(10)$; (c) Relative change in $H_2(10)$; (d) Relative change in $M_1(10)$; (e) Relative change in $M_2(10)$. The baseline parameters are those shown in the caption of Fig. 12. (For interpretation of the references to color in this figure legend, the reader is referred to the web version of this article.)

are some studies on the interactions between macrophages and $CD4^+$ T cells, for example, in the context of breast and lung cancer (DeNardo et al., 2009; Almatroodi et al., 2016), or in the context of rheumatoid arthritis (Roberts et al., 2015), such studies do not shed much light on the nonlinear interactions between these different types of immune cells.

In the context of the anti-tumour effect of macrophages, the sensitivity analysis in Fig. 14(a) suggested that tumour elimination was mainly the effect of M1 macrophages (and to a lesser extent the effect of Th1 cells). This is an interesting hypothesis generated by the model, which, if validated experimentally, could influence the current anti-tumour immune therapies that focus mainly on T cell responses (Wang et al., 2014; Voena and Chiarle, 2016). In contrast, the sensitivity analysis in Fig. 15 suggested that the transient decrease in tumour size on day 10 during tumour dormancy was mainly the effect of Th1 cells (and to a lesser extent the effect of M1 cells). In fact, the tumour dormant behaviour was the result of a delicate balance between the anti-tumour responses of Th1 and M1 cells, and the pro-tumour responses of M2 cells. In addition, the results in Figs. 8 and 9 suggested that the three parameters, g_{H_1}, g_{M_1} and g_{M_2}, influenced also the asymptotic behaviour of model (3). This is in support of the idea that anti-cancer immunotherapies should focus on the combined effect of T cells and M1 macrophages.

The results in Fig. 8 suggested that there could be very few M2 cells (and many M1 and Th1 cells), but if these M2 cells secrete large amounts of type-II cytokines (i.e., large g_{M_2}), they can skew the tumour microenvironment in favour of tumour sustenance and growth. This would support the experimental results in Mattes et al. (2003), where a type-I environment was not enough to eliminate B16F10 melanoma cells. The authors in Mattes et al. (2003) recognised that the inability of Th1 cells to eradicate tumours might have been influenced by the presence of pro-angiogenic tumour-infiltrating macrophages (i.e., M2 cells), but they did not measure the levels of M2 and M1 macrophages, nor the levels of Th1 and Th2 cells. In fact, Mattes et al. (2003) identified the Th1 and Th2 immune responses by the levels of type-I and type-II cytokines produced by these cells: high IL-5, IL-13 and IL-4 for a Th2-dominated response, and high IFN-γ, TNF-α and IL-13 for a Th1-dominated response (note here the relatively high levels of IL-13 observed during both Th1 and Th2 responses; and the fact that IL-13 is also involved in the alternative activation of M2 macrophages (Martinez and Gordon, 2014)). Since many experimental studies focus on the levels of cytokines as a proxy for the number of immune cells corresponding to a type-I or type-II response (Mattes et al., 2003; Almatroodi et al., 2016), to be able to test our hypothesis regarding the role of g_{H_2} and M2 cells on tumour persistence during type-I responses, we need to extend model (3) by incorporating explicitly the effects of type-I and type-II cytokines on tumour-immune interactions (i.e., an approach similar to Eftimie et al. (2010), where a mathematical models

incorporated the effects of type-I, type-II, tumour-promoting and tumour-suppressing cytokines).

In this study, to keep the models relatively simple, we ignored deliberately the microenvironment which can alter the immune response against cancer (Hanahan and Weinberg, 2011). However, the incorporation of the explicit effects of type-I and type-II cytokines (which can be further altered by the tumour cells (Burkholder et al., 2014)) would allow us not only to compare our results with available experimental cytokine data, but also to gain a better understanding of how to control cell-cell communication (by controlling cytokine signalling) with the ultimate goal of improving cancer immunotherapies.

Note from Table A.1 that models (1) and (3) contain both fast and slow variables. One could have used a quasi-steady state analysis to simplify the models. However, such an analysis might lead to limitations in our understanding of the transient dynamics of the Th1-Th2 and M1-M2 cells (see, for example the study in Flach and Schnell (2006)). This type of transient dynamics was observed in experimental studies on early tumour behaviours, which suggested that the ratios of Th1/Th2 cells or M1/M2 cells can be used as independent predictive markers of patient survival (Monte et al., 2011; Protti and Monte, 2012; Chen et al., 2011). In this theoretical study we showed that these ratios of immune cells can change once or twice before they stabilise towards a steady state (and they stabilise when the tumour reaches either a very large size or is eliminated; see Figs. 10–12). The changes in the dominating Th or macrophages dynamics are not always correlated with each other. Moreover, we showed the possibility of having a long-term oscillatory tumour-immune dynamics characterised by low tumour values and periodic changes between type-I and type-II immune responses; see Fig. 13. While sustained periodic tumour oscillations are not very often observed in clinical studies (although see Gliozzi et al., 2010), we emphasise that model (3) exhibits such oscillations for tumour sizes around the detection threshold (of about $10^7 - 10^8$ cells (Friberg and Mattson, 1997)). This suggest that oscillations between type-I and type-II immune responses (in the presence of tumour) might be more common in clinical/experimental settings but they might not be measured since the tumour cannot be detected. Overall, we hypothesise that trying to predict the long-term outcome of the tumour while the ratios Th1/Th2 and M1/M2 are still varying due to the cross-talk with the tumour environment, might not always offer accurate predictions on patient survival.

At a more theoretical level, it would be interesting to investigate the differences between the double feedback in tumour-immune dynamics modelled in this study, and a single feedback for tumour-immune interactions. Such an investigation (to be the subject of a future study) would allow us to uncover the minimal biological mechanisms that need to be incorporated into a model to explain the dominant type-I and/or type-II immune responses associated with cancer immunotherapies.

Finally, these numerical results for systems (1) and (3) have generated two new mathematical questions that will be answered analytically in future studies: (i) analytical investigation of fast and slow parameters that control transient and long-term tumour-immune behaviours, and how the simplified dynamics in the slow/fast models matches the original dynamics; (ii) analytical investigation of the Hopf bifurcation that generated the limit cycle shown in Fig. 13.

Biological realism of the parameter values and overall results. The results of this study depend on the parameter values described in Table A.1. Some of these values were taken from the literature, others were approximated based on published experimental results, and the remaining values were varied within some estimated ranges (see Appendix A). This approach is very common in the mathematical immunology literature, due to a lack of quantitative results regarding the immune responses following various antigen stimulations. In addition to the fact that very few labs measure and estimate kinetic parameters (the majority of such studies focusing on lymphocyte kinetics following pathogen stimulation; see for example Borghans and Boer, 2007; Asquith et al., 2009; Boer and Perelson, 2013), there is also the difficulty of interpreting kinetic data; see the review in Boer and Perelson (2013). Moreover, the few rigorously estimated kinetic parameters in the mathematical immunology literature depend on the estimation method used, as emphasised in Laydon et al. (1675). A more detailed discussion on model validation and parameter estimation in mathematical immunology can be found in Eftimie et al. (2016).

Based on these facts, we acknowledge that the majority of models in the mathematical immunology literature, including this particular study, can have at this moment only a theoretical value. In particular, the model presented here can only propose hypotheses regarding the possible outcomes of the interactions between the Th1-Th2 and M1-M2 immune responses, in the absence/presence of tumour cells.

We showed that small variations in the values of parameters that control tumour cells lysis via anti-tumour cytokines (e.g., g_{H_1}, g_{M_1}, g_{M_2}), or the parameters for the activation of Th cells (a_{H_1}, a_{H_2}), or the macrophages re-polarisation rates (r_{M_1}, r_{M_2}) could explain the variety of tumour-immune dynamics observed in the experimental literature. To obtain a better understanding of immune responses to specific diseases, the next step would be to quantify the rates that control various type-I and type-II immune responses. Therefore, for a better mechanistic understanding of the *in vivo* immune responses, which can be obtained with a more realistic *in silico* model, mathematicians (and immunologists) need to have access to relevant experimental data that could then be used to parametrise the mathematical models. The goal of our present study was not to parametrise the models to specific diseases, but to propose some general hypotheses regarding the processes involved in different immune responses.

Acknowledgements

RE acknowledges partial support from an Engineering and Physical Sciences Research Council (UK) First Grant number EP/K033689/1, and from a Northern Research Partnership (Scotland) grant.

Appendix A. Parameter values

In Table A.1 we summarise the parameter values used throughout this theoretical study. Some of these values were taken directly from existent mathematical literature, while other values were approximated based on experimental studies (marked by "*" in Table A.1); see also the discussion below. However, there were a few parameters for which we could not find any values, so we had to provide estimates for them. Some of these estimates were varied within specified ranges (see Table A.1).

Next, we discuss the parameter values we approximated using experimental studies, and the values taken from the literature (especially if different mathematical studies used different parameter values).

- Danciu et al. (2013) have shown that melanoma cells have a doubling time between 17.2 h and 24 h, which corresponds to a tumour growth rate of $0.69 - 0.97$. For simplicity, throughout this study we choose $\alpha = 0.69/\text{day}$.

- The proliferation of Th1 and Th2 cells occurs in the presence of type-1 and type-2 cytokines produced by the cells themselves and by the macrophages in the environment. For simplicity (and since we could not find data on the interactions between cytokines and cells; i.e., interaction radii, concentration of molecules that lead to cell proliferation), we assume that: (i) the concentrations of type-1 and type-2 cytokines are directly proportional to the density of M1 and M2 cells, and (ii) the interaction rates between cells and cytokines, p_{H_1} and p_{H_2}, are the same for both populations. This assumption is consistent with the approach in Kogan et al. (2013), Eftimie et al. (2010), which consider similar recruitment rates for the Th1 and Th2 cells, in response to the cytokine environment. Due to a lack of consistent data on the growth of Th1 and Th2 populations (e.g., Eftimie et al. (2010) assumed a growth rate of 0.09, while Kogan et al. (2013) assumed a growth rate between $10^2 - 10^4$), in this study, we used an estimated interaction rate of $p_{H_1} = p_{H_2} = 0.09$. Note that in Fig. 14 we performed a sensitivity analysis of model dynamics to changes in parameter values, and investigated also the effect of variations in p_{H_1} and p_{H_2}.
- In regard to macrophages apoptosis rate, Magombedze et al. (2014) used a death rate of 0.02/day. On the other hand Wang et al. (2012) used a death rate of 0.2/day. However, experimental studies in Gauthier et al. (2013) showed that mice macrophages were cleared within 5-8 days of induction of inflammation, during the resolution stage of inflammation. However, since inflammation is a critical component of tumour progression (Cousins and Werb, 2002), and we could not find any specific references regarding the half-life of macrophages inside tumours, we assumed here that the death rate of tumour macrophages is much lower than in Wang et al. (2012), and more similar to the value in Magombedze et al. (2014): $e_{M_1} = e_{M_2} = 0.02$/day.
- In regard to the proliferation of macrophages, Jenkins et al. (2011) showed that by treating M2 macrophages with 5 μg of IL-4 and 25 μg anti-IL-4 antibody (to extend the half-life of the cytokine), it leads to an increased proliferation of macrophages 4 days later (from 1×10^6 in the control case to about 4.2×10^6 in the IL-4 case). We can approximate the interaction rate between M2 macrophages and the IL-4 cytokine concentration (produced by Th2 cells) as $p_{M_2} = \ln(4.2)/(4 \times 30\mu g) = 0.012$. Assuming only $5\mu g$ of IL-4, it leads to $p_{M_2} = \ln(4.2)/(4 \times 5\mu g) = 0.072$. Throughout this study we consider an average of $p_{M_2} = 0.02$ (obtained assuming $17.5\,\mu g$ of IL-4 in the system). For the self-proliferation rate of M1 macrophages, we could not find any data. For simplicity, throughout the simulations we used an average value $p_{M_1} = 0.02$. Nevertheless, in Fig. 14 we also investigated the sensitivity of tumour growth in response to changing $p_{M_1} \in (0.002, 0.038)$.
- In Lee et al. (1985) it was suggested that a conservative estimate for the total number of macrophages in a normal adult mouse would be greater than 1×10^8. Therefore, we have chosen the macrophages carrying capacity to be $m_2 = 10^9$.
- In the mathematical literature there are various estimations for tumour natural death rate. For example, Wang et al. (2015) estimated a value of 2.08×10^{-6}/day, while Wodarz et al. (2004) used arbitrary units and estimated tumour death rate at 0.1. On the other hand, Moore and Li (2004) considered a tumour cell death rate within the range (0,0.8)/day. Since apoptosis is inactivated in cancer cells (Brown and Attardi, 2005), in this study, we use an estimated value of natural death rate for cancer cells of $f = 10^{-8}$/day.
- In regard to the tumour killing rates by Th1 and Th2 cells (via the cytokines they produce), we note that Hung et al. (1998) incubated 10^6 B16 melanoma cells with CD4 T cells. The maximum tumour lysis was 30%, obtained at an effector: target ratio of about 32:1. This corresponds to a tumour killing rate of $g_{H1}, g_{H2} = 5.3 \times 10^{-8}$ (den Breems and Eftimie, 2016). Throughout this study, we investigate what happens with the dynamics of model (3) when we vary $g_{H1}, g_{H2} \in (10^{-9}, 10^{-7})$.
- Various mathematical studies that investigated macrophages dynamics considered an activation rate within the range (0.0-1.0)/day, depending on the concentration of type-I and type-II cytokines that trigger their activation (Wigginton and Kirschner, 2001; Wang et al. (2012)). However, the activation of M1 macrophages is reduced in the presence of type-II cytokines such as IL-10 (Wigginton and Kirschner, 2001), and the activation of M2 macrophages is reduced in the presence of type-I cytokines such as IFN-γ (Wang et al., 2012). Since the tumour environment contains both type-I and type-II cytokines, throughout this study we consider lower estimates for the macrophages activation rates: $a_{M1}, a_{M2} = 0.001$.

Appendix B. Non-negative solutions

Here, we show that system (3) has non-negative solutions. Since (3) is a generalisation of (1), the results hold also for model (1).

To start, we assume that $T(0), H_1(0), H_2, M_1(0), M_2(0) \geq 0$. Note that if $T(0) = 0$, $M_1(0) = 0$, $M_2(0) = 0$, $H_1(0) = 0$, $H_2(0) = 0$, then the system is at equilibrium and the only solution is the trivial one.

Assume that it is possible to have negative solutions. Then there exists a time $t_0 < \infty$ defined as

$$t_0 = \inf\{t > 0 | T(t) < 0, H_1(t) < 0, H_2(t) < 0, M_1(t) < 0, \quad \text{or } M_2(t) < 0\}. \tag{B.1}$$

We have the following inequalities:

- From Eq. (3a):

$$\frac{dT}{dt} \geq -T(f + g_{H_1}H_1 + g_{H_2}H_2 + g_{M_1}M_1 - g_{M_2}M_2), \quad \text{for} \quad t \leq t_0. \tag{B.2}$$

Since $T(t_0) \geq 0$, there exists a non-negative solution $T(t) \geq T(t_0)e^{-\int(f+g_{H_1}H_1+g_{H_2}H_2+g_{M_1}M_1-g_{M_2}M_2)ds} \geq 0$, for $t \in (t_0 - \epsilon_1, t_0 + \epsilon_1)$.

- From Eq. (3b):

$$\frac{dH_1}{dt} \geq -H_1(n_{H_1}T + e_{H_1}), \quad \text{for} \quad t \leq t_0. \tag{B.3}$$

Since $H_1(t_0) \geq 0$, there exists a non-negative solution $H_1(t) \geq H_1(t_0)e^{-\int(n_{H_1}T+e_{H_1})ds} \geq 0$, for $t \in (t_0 - \epsilon_2, t_0 + \epsilon_2)$.

- From Eq. (3c):

$$\frac{dH_2}{dt} \geq -H_2(n_{H_2} + e_{H_2}), \quad \text{for} \quad t \leq t_0. \tag{B.4}$$

Since $H_2(t_0) \geq 0$, there exists a non-negative solution $H_2(t) \geq H_2(t_0)e^{-\int(n_{H_2}T+e_{H_2})ds} \geq 0$, for $t \in (t_0 - \epsilon_3, t_0 + \epsilon_3)$.

- From Eq. (3d):

$$\frac{dM_1}{dt} \geq -M_1(n_{M_1}T + e_{M_1} + r_{M_2}), \quad \text{for} \quad t \leq t_0. \tag{B.5}$$

Since $M_1(t_0) \geq 0$, there exists a non-negative solution $M_1(t) \geq M_1(t_0)e^{-\int(n_{M_1}T+e_{M_1}+r_{M_2})ds} \geq 0$, for $t \in (t_0 - \epsilon_4, t_0 + \epsilon_4)$.

- From Eq. (3e):

$$\frac{dM_2}{dt} \geq M_2(n_{M_2}T - e_{M_2} - r_{M_1}), \quad \text{for} \quad t \leq t_0. \tag{B.6}$$

Since $M_2(0) \geq 0$, there exists a non-negative solution $M_2(t) \geq M_2(t_0)e^{\int(n_{M_2}T-e_{M_2}-r_{M_1})ds} \geq 0$, for $t \in (t_0 - \epsilon_5, t_0 + \epsilon_5)$.

Therefore, the solution (T, H_1, H_2, M_1, M_2) of system (3) is nonnegative for $t \in [t_0, t_0 + \epsilon)$, with $\epsilon = \min\{\epsilon_1, \epsilon_2, \epsilon_3, \epsilon_4, \epsilon_5\}$, which contradicts the initial assumption on t_0. Therefore, the solution remains non-negative for all time.

Appendix C. Model non-dimensionalisation

In the following, we present the non-dimensional versions of model (3) (since model (3) is a generalisation of model (1), we choose not to present also the non-dimensional version of (1)). Consider the following scaling for the variables and parameters that appear in these two models:

$$\bar{t} = t\frac{a_{H1}m_2}{m_1}, \quad \overline{H_1} = \frac{H_1}{m_1}, \quad \overline{H_2} = \frac{H_2}{m_1}, \quad \overline{M_1} = \frac{M_1}{m_2}, \quad \overline{M_2} = \frac{M_2}{m_2}, \quad \overline{T} = \frac{T}{\beta}, a_1 = \frac{a_{H_2}}{a_{H_1}}, \quad a_2 = \frac{a_{M_1}m_1^2}{a_{H_1}m_2^2}, \quad a_3 = \frac{a_{M_2}m_1^2}{a_{H_1}m_2^2}, \quad b_1 = \frac{p_{H_1}m_1}{a_{H_1}}, \quad b_2 = \frac{p_{H_2}m_1}{a_{H_1}},$$

$$b_3 = \frac{p_{M_1}m_1}{a_{H_1}m_2}, b_4 = \frac{p_{M_2}m_1^2}{a_{H_1}m_2}, \quad e_1 = \frac{e_{H_1}m_1}{a_{H_1}m_2}, \quad e_2 = \frac{e_{H_2}m_1}{a_{H_1}m_2}, \quad e_3 = \frac{e_{M_1}m_1}{a_{H_1}m_2}, \quad e_4 = \frac{e_{M_2}m_1}{a_{H_1}m_2}, r_1 = \frac{r_{M_1}m_1}{a_{H_1}m_2}, \quad r_2 = \frac{r_{M_2}m_1}{a_{H_1}m_2}, \quad n_1 = \frac{n_{H_1}\beta m_1}{a_{H_1}m_2}, \quad n_2 = \frac{n_{H_2}\beta m_1}{a_{H_1}m_2},$$

$$n_3 = \frac{n_{M_1}\beta}{a_{H_1}}, \quad n_4 = \frac{n_{M_2}\beta}{a_{H_1}}, f_1 = \frac{\alpha m_1}{a_{H_1}m_2}, \quad f_2 = \frac{g_{H_1}m_1^2}{a_{H_1}m_2}, \quad f_3 = \frac{g_{H_2}m_1^2}{a_{H_1}m_2}, \quad f_4 = \frac{g_{M_1}m_1}{a_{H_1}}, \quad f_5 = \frac{g_{M_2}m_1}{a_{H_1}}, \quad f_6 = \frac{fm_1}{a_{H_1}m_2}.$$

After dropping the bar for simplicity, we obtain the following equations for the time-evolution of variables describing the tumour and immune cells (i.e., the non-dimensional version of model (3)):

$$\frac{dT}{dt} = f_1T(1-T) - f_2H_1T - f_3H_2T - f_4M_1T + f_5M_2T - f_6T, \tag{C.1a}$$

$$\frac{dH_1}{dt} = M_1 + b_1H_1M_1(1 - H_1 - H_2) - n_1H_1T - e_1H_1, \tag{C.1b}$$

$$\frac{dH_2}{dt} = a_1M_2 + b_2H_2M_2(1 - H_1 - H_2) - n_2H_2T - e_2H_2, \tag{C.1c}$$

$$\frac{dM_1}{dt} = a_2H_1 + b_3M_1(1 - M_1 - M_2) - n_3M_1T - e_3M_1 + r_1M_2 - r_2M_1, \tag{C.1d}$$

$$\frac{dM_2}{dt} = a_3H_2 + b_4M_2H_2(1 - M_1 - M_2) + n_4M_2T - e_4M_2 - r_1M_2 + r_2M_1. \tag{C.1e}$$

Since this non-dimensionalisation approach did not lead to a significant reduction in model parameters (i.e., the 31 parameters in model (3), were reduced to 25 parameters in model (C.1)), we prefer to work with the original dimensional model. Moreover, while a sensitivity analysis could be performed on the non-dimensional parameters shown above, such an analysis would not shed light on the effect of original parameters/rates on tumour growth (especially since parameters such as m_1 and m_2 - important for the sensitivity of the original model - enter in various combination terms that form the non-dimensional parameters).

Appendix D. Bifurcation diagrams for the dominant immune responses

Consider the ratios of the steady states M_1^*/M_2^* and H_1^*/H_2^* given by (2):

$$\frac{M_1^*}{M_2^*} = \frac{e_{H_1}H_1^*\left(a_{H_2} + p_{H_2}H_2^*\left(1 - \frac{H_1^* + H_2^*}{m_1}\right)\right)}{e_{H_2}H_2^*\left(a_{H_1} + p_{H_1}H_1^*\left(1 - \frac{H_1^* + H_2^*}{m_1}\right)\right)}, \tag{D.1}$$

$$\frac{H_1^*}{H_2^*} = \frac{\left(a_{M_2} + p_{M_2}M_2^*\left(1 - \frac{M_1^* + M_2^*}{m_2}\right)\right)\left(e_{M_1}M_1^* + r_{M_2}M_1^* - r_{M_1}M_2^* - p_{M_1}M_1^*\left(1 - \frac{M_1^* + M_2^*}{m_2}\right)\right)}{e_{M_2}M_2^* + r_{M_1}M_2^* - r_{M_2}M_1^*}. \tag{D.2}$$

Numerical simulations show that, at the steady state, $M_1^* + M_2^* \approx m_2$ and $H_1^* + H_2^* \approx m_1$ (see also Figs. 6 and 7). In this case, the previous two ratios reduce to

$$\frac{M_1^*}{M_2^*} = \frac{e_{H_1}H_1^*a_{H_2}}{e_{H_2}H_2^*a_{H_1}}, \quad \frac{H_1^*}{H_2^*} = \frac{a_{M_2}(e_{M_1}M_1^* + r_{M_2}M_1^* - r_{M_1}M_2^*)}{e_{M_2}M_2^* + r_{M_1}M_2^* - r_{M_2}M_1^*}. \tag{D.3}$$

Solving the first equation in (D.3) for $H_1^*/H_2^* = (M_1^*/M_2^*)(a_{H_1}/a_{H_2})(e_{H_2}/e_{H_1})$, and substituting this term into the second equation in (D.3), denoting by $M^* = M_1^*/M_2^*$, $r_M = r_{M_1}/r_{M_2}$ and $a_H = a_{H_1}/a_{H_2}$, leads to the following second order equation in M^*:

$$a_H a_M \left(\frac{e_{H_2}}{e_{H_1}}\right)\left(M^*\frac{e_{M_2}}{r_{M_2}} + r_M M^* - M^{*2}\right) = \frac{e_{M_1}}{r_{M_2}}M^* - r_M + M^*. \tag{D.4}$$

If we fix r_{M_2} and vary r_{M_1}, we can graph implicitly M^* versus r_M versus a_H (or a_M), as shown in Fig. 5.

Consider now model (3). The case of the tumour-free steady state follows the previous case, and the changes in the immune response as we vary a_{H_1}/a_{H_2} or r_{H_1}/r_{H_2} can be described again by Fig. 5.

Now, we focus on the steady state (4), and discuss the parameter range where this tumour-present state exists. We look for solutions $T^* > 0$ of

$$\alpha - T^*\frac{\alpha}{\beta} - f - g_{H_1}H_1^* - g_{H_2}H_2^* - g_{M_1}M_1^* + g_{M_2}M_2^* = 0. \tag{D.5}$$

Using (4b)–(4d), we can replace H_1^* and H_2^* by M_1^*, M_2^* and T^*. Again we make the assumption that $M_1^* + M_2^* \approx m_2$, $H_1^* + H_2^* \approx m_1$, as seen numerically for the steady state dynamics of these models (see also Figs. 10 and 11). Finally, re-writing $M_{1,2}^*$ in terms of m_2 and $M^* = M_1^*/M_2^*$ we obtain the implicit Eq. (6), whose solution was graphed in Fig. 8(a)–(c) (left panels) for different values of g_{M_2} versus M^*. One could also graph g_{M_2} versus $H^* = H_1^*/H_2^*$ (right panels in Fig. 8), by considering the relation between the ratio of Th1 and Th2 cells in the presence of tumour cells:

$$\frac{H_1^*}{H_2^*} = \left(\frac{M_1^*}{M_2^*}\right)\left(\frac{a_{H_1}}{a_{H_2}}\right)\left(\frac{n_{H_2}T^* + e_{H_2}}{n_{H_1}T^* + e_{H_1}}\right). \tag{D.6}$$

Appendix E. Jacobian matrix for the immune and tumour-immune systems

The Jacobian matrix associated with system (1) is:

$$J_1 = \begin{pmatrix} a_{11} & a_{12} & a_{13} & a_{14} \\ a_{21} & a_{22} & a_{23} & a_{24} \\ a_{31} & a_{32} & a_{33} & a_{34} \\ a_{41} & a_{42} & a_{43} & a_{44} \end{pmatrix} \tag{E.1}$$

with

$$a_{11} = p_{H_1}M_1^*\left(1 - \frac{H_1^* + H_2^*}{m_1}\right) - \frac{p_{H_1}H_1^*M_1^*}{m_1} - e_{H_1}, \quad a_{12} = -\frac{p_{H_1}H_1^*M_1^*}{m_1}, \; a_{13} = a_{H_1} + p_{H_1}H_1^*\left(1 - \frac{H_1^* + H_2^*}{m_1}\right), \quad a_{14} = 0,$$

$$a_{21} = -\frac{p_{H_2}H_2^*M_2^*}{m_1}, \; a_{22} = p_{H_2}M_2^*\left(1 - \frac{H_1^* + H_2^*}{m_1}\right) - \frac{p_{H_2}H_2^*M_2^*}{m_1} - e_{H_2}, \quad a_{23} = 0, \quad a_{24} = a_{H_2} + p_{H_2}H_2^*\left(1 - \frac{H_1^* + H_2^*}{m_1}\right), \; a_{31} = a_{M_1}, \quad a_{32} = 0,$$

$$a_{33} = p_{M_1}\left(1 - \frac{M_1^* + M_2^*}{m_2}\right) - \frac{p_{M_1}M_1^*}{m_2} - e_{M_1} - r_{M_2}, \; a_{34} = -\frac{p_{M_1}M_1^*}{m_2} + r_{M_1}, \quad a_{41} = 0, \quad a_{42} = a_{M_2} + p_{M_2}M_2^*\left(1 - \frac{M_1^* + M_2^*}{m_2}\right),$$

$$a_{43} = -\frac{p_{M_2}M_2^*H_2^*}{m_2} + r_{M_2}, \; a_{44} = p_{M_2}H_2^*\left(1 - \frac{M_1^* + M_2^*}{m_2}\right) - \frac{p_{M_2}M_2^*H_2^*}{m_2} - e_{M2} - r_{M_1}.$$

Fig. E.16 shows the stability of the steady states exhibited by model (1) as we vary one parameter. For simplicity, we chose parameter $r_{M_1} \in [0.05, 0.09]$ (but we note that we could have chosen any other parameter). The four symbols in Fig. E.16 show the real parts of the four eigenvalues corresponding to the Jacobian matrix (E.1). Numerical calculations of the eigenvalues corresponding to the steady state (0, 0, 0, 0) show that this state is stable for the parameter values shown in Table A.1. In regard to the two immune coexistence steady states (H_1^*, H_2^*, M_1^*, M_2^*)

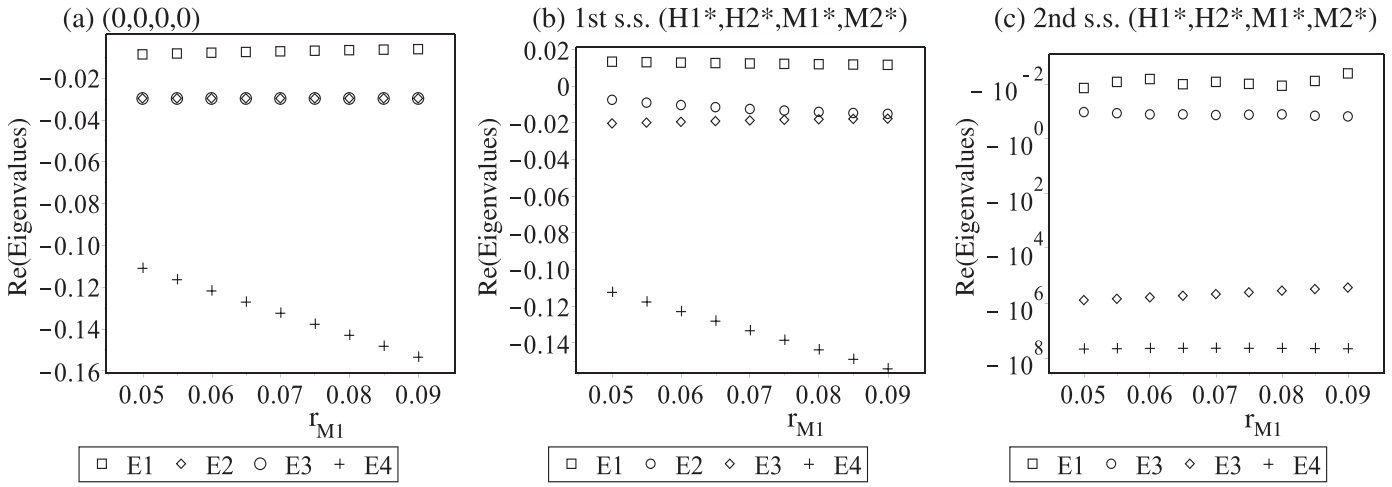

Fig. E.16. Eigenvalues $E1 - E4$ of the Jacobian matrix (E.1) calculated at 3 different steady states: (a) Zero state (0, 0, 0, 0);(b) first coexistence state (H_1^*, H_2^*, M_1^*, M_2^*); (c) second coexistence state (H_1^*, H_2^*, M_1^*, M_2^*). Here we assume that $a_{H_1} = a_{H_2} = 0.001$, $r_{M_2} = 0.05$ and $r_{M_1} \in [0.05, 0.09]$. The rest of parameter values are as described in Table A.1.

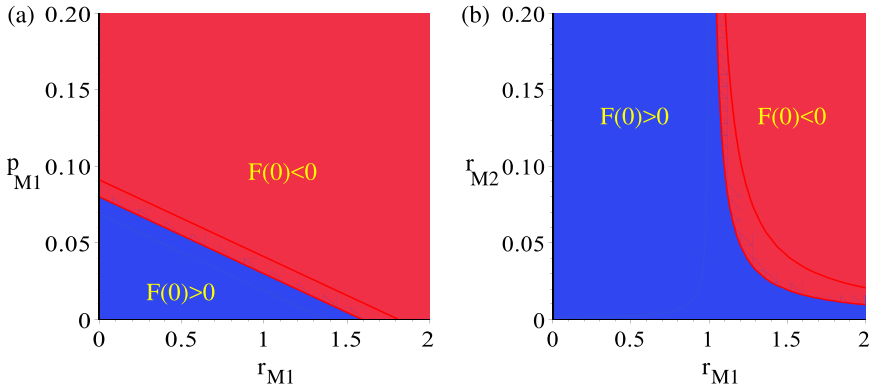

Fig. E.17. Example of parameter regions where the steady state (0, 0, 0, 0) can be unstable (i.e., $F(0) < 0$). (a) (r_{M_1}, p_{M_1}) plane; (b) (r_{M_1}, r_{M_2}) plane. All other parameters are kept fixed as in Table A.1.

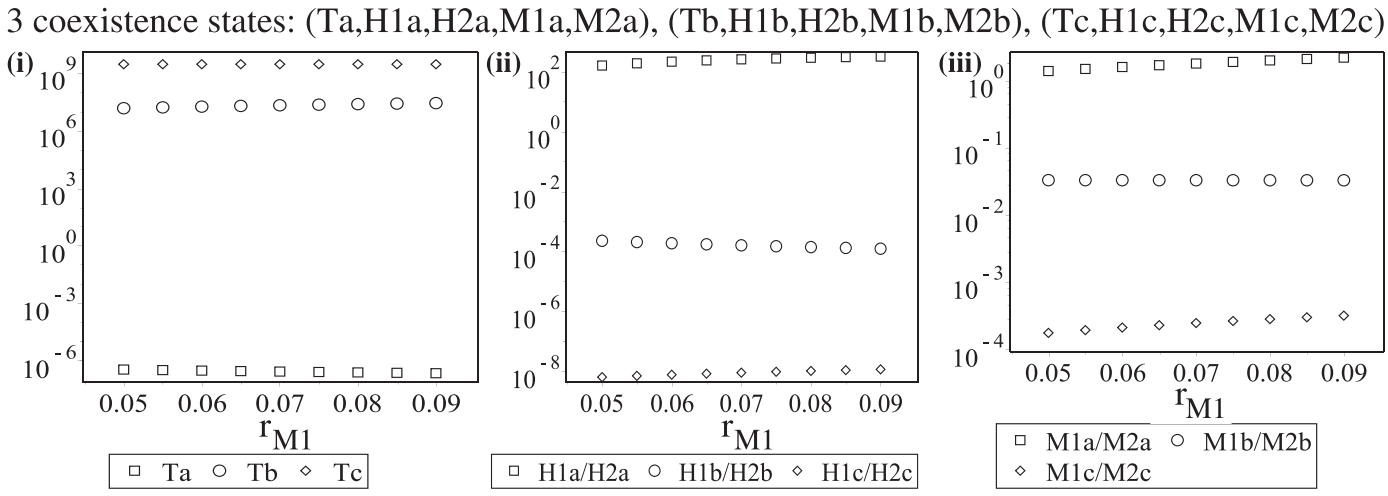

Fig. E.18. There tumour-immune coexistence states (T^*, H_1^*, H_2^*, M_1^*, M_2^*) exhibited by model (3): (a) values of tumour sizes T^*; (b) values of ratios H_1^*/H_2^* corresponding to the 3 tumours sizes depicted in (a); (c) values of ratios M_1^*/M_2^* corresponding to the 3 tumours sizes depicted in (a). Here we assume that $g_{M_2} = 2.3 \times 10^{-10}$, $g_{H_1} = 5 \times 10^{-9}$, $a_{H_1} = a_{H_2} = 0.001$, $r_{M_2} = 0.05$ and $r_{M_1} \in [0.05, 0.09]$. The rest of parameter values are as described in Table A.1.

depicted in Fig. 4: the state with low immune response (point (i) on Fig. 4) is unstable, as shown in Fig. E.16(b), and the state with high immune response (point (ii) on Fig. 4) is stable, as shown in Fig. E.16(c).

We need to emphasise that these stability results depend strongly on all other parameter values listed in Table A.1. As an example, in the following we show analytically how the stability of the zero state (0, 0, 0, 0) depends on the various parameters in the system. (While such an analysis could be also performed for all other steady states, it is too complicated and beyond the scope of this paper). The characteristic equation associated with $\det(J_{(0,0,0,0)} - \lambda \mathbb{I}) = 0$ is given by

$$0 = (-e_{H_1} - \lambda)\Big[(-e_{H_2} - \lambda)(p_{M_1} - e_{M_1} - r_{M_2} - \lambda)(-e_{M_2} - r_{M_1} - \lambda) + r_{M_1} r_{M_2}(e_{H_2} + \lambda) - a_{H_2} a_{M_2}(p_{M_1} - e_{M_1} - r_{M_2} - \lambda)\Big]$$
$$+ a_{H_1}[a_{M_1} a_{M_2} a_{H_2} - a_{M_1}(e_{H_2} + \lambda)(e_{M_2} + r_{M_1} + \lambda)] = F(\lambda).$$

Note that this 4^{th} order polynomial in λ (let us call it $F(\lambda)$) can have up to 4 real roots. For $\lambda \to \pm\infty$, we have $F(\lambda) \to \infty$. If we can show that there are parameter values for which, at $\lambda = 0$ we have $F(0) < 0$, then it becomes clear that one root λ must be positive (and thus the zero-state becomes unstable).

$$F(0) = -e_{H_1}\Big[(-e_{H_2})(p_{M_1} - e_{M_1} - r_{M_2})(-e_{M_2} - r_{M_1}) + r_{M_1} r_{M_2}(e_{H_2}) - a_{H_2} a_{M_2}(p_{M_1} - e_{M_1} - r_{M_2})\Big] + a_{H_1}[a_{M_1} a_{M_2} a_{H_2} - a_{M_1}(e_{H_2})(e_{M_2} + r_{M_1})]$$

It is easy to observe that large r_{M_1}, r_{M_2} or p_{M_1} values can all lead to $F(0) < 0$. Fig. E.17 shows two possible parameter regions where $F(0) < 0$, thus ensuring that at least one eigenvalue λ of the Jacobian matrix $J_1(0, 0, 0, 0)$ is positive and the zero state is unstable.

The Jacobian matrix associated with system (3) is:

$$J_2 = \begin{pmatrix} b_{11} & b_{12} & b_{13} & b_{14} & b_{15} \\ b_{21} & b_{22} & b_{23} & b_{24} & b_{25} \\ b_{31} & b_{32} & b_{33} & b_{34} & b_{35} \\ b_{41} & b_{42} & b_{43} & b_{44} & b_{45} \\ b_{51} & b_{52} & b_{53} & b_{54} & b_{55} \end{pmatrix} \quad \text{(E.2)}$$

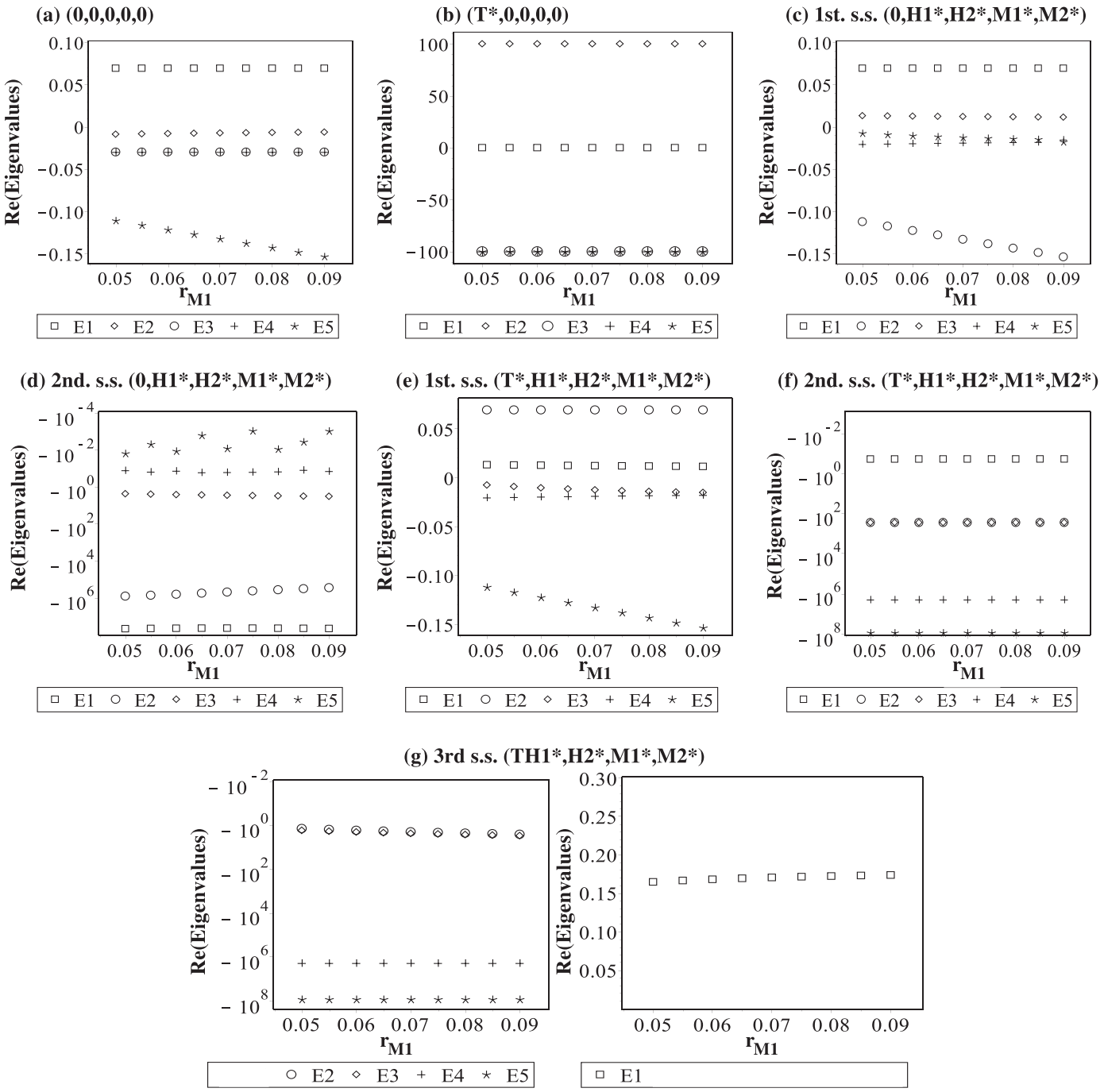

Fig. E.19. The real part of eigenvalues E1-E5 of the Jacobian matrix (E.1) calculated at 3 different steady states: (a) Zero state (0, 0, 0, 0, 0);(b) Tumour-present, immune-absent state: ($T^* = \beta(1 - f/\alpha)^*$, 0, 0, 0, 0); (c), (d) Two tumour-absent, immune-present states: (0, H_1^*, H_2^*, M_1^*, M_2^*); (e), (f)(g) Three tumour-immune coexistence states: (T^*, H_1^*, H_2^*, M_1^*, M_2^*). Here we assume that $g_{M_2} = 2.3 \times 10^{-10}$, $g_{H_1} = 5 \times 10^{-9}$, $a_{H_1} = a_{H_2} = 0.001$, $r_{M_2} = 0.05$ and $r_{M_1} \in [0.05, 0.09]$. The rest of parameter values are as described in Table A.1.

with

$$b_{11} = \alpha(1 - \frac{T^*}{\beta}) - \frac{\alpha T^*}{\beta} - g_{H_2}H_2^* - g_{M_1}M_1^* + g_{M_2}M_2^*, \quad b_{12} = -g_{H_1}, \quad b_{13} = -g_{H_2}T^*, b_{14} = -g_{M_1}T^*, \quad b_{15} = g_{M_2}T^*, b_{21} = -n_{H_1}H_1^*,$$

$$b_{22} = p_{H_1}M_1^*(1 - \frac{H_1^* + H_2^*}{m_1}) - \frac{p_{H_1}H_1^*M_1^*}{m_1} - e_{H_1} - n_{H_1}T^*, \quad b_{23} = -\frac{p_{H_1}H_1^*M_1^*}{m_1}, b_{24} = a_{H_1} + p_{H_1}H_1^*(1 - \frac{H_1^* + H_2^*}{m_1}), \quad b_{25} = 0,$$

$$b_{31} = -n_{H_2}H_2^*, \quad b_{32} = -\frac{p_{H_2}H_2^*M_2^*}{m_1}, \quad b_{33} = p_{H_2}M_2^*\left(1-\frac{H_1^*+H_2^*}{m_1}\right) - \frac{p_{H_2}H_2^*M_2^*}{m_1} - e_{H_2} - n_{H_2}T^*, \; b_{34} = 0,$$

$$b_{35} = a_{H_2} + p_{H_2}H_2^*\left(1-\frac{H_1^*+H_2^*}{m_1}\right), \; b_{41} = -n_{M_1}M_1^*, \quad b_{42} = a_{M_1}, \quad b_{43} = 0,$$

$$b_{44} = p_{M_1}\left(1-\frac{M_1^*+M_2^*}{m_2}\right) - \frac{p_{M_1}M_1^*}{m_2} - n_{M_1}T^* - e_{M_1} - r_{M_2}, \; b_{45} = -\frac{p_{M_1}M_1^*}{m_2} + r_{M_1}, \; b_{51} = n_{M_2}M_2^*, \quad b_{52} = 0, \quad b_{53} = a_{M_2} + p_{M_2}M_2^*\left(1-\frac{M_1^*+M_2^*}{m_2}\right),$$

$$b_{54} = -\frac{p_{M_2}M_2^*H_2^*}{m_2} + r_{M_2}, \; b_{55} = p_{M_2}H_2^*\left(1-\frac{M_1^*+M_2^*}{m_2}\right) - \frac{p_{M_2}M_2^*H_2^*}{m_2} - e_{M2} - r_{M_1} + n_{M_2}T^*.$$

Note that system (3) has: (i) one trivial steady state (0,0,0,0,0); (ii) one tumour-present, immune-absent state ($T^* = \beta - \beta f/\alpha$, 0, 0, 0, 0); (iii) two tumour-absent, immune-present states: (0, H_1^*, H_2^*, M_1^*, M_2^*), similar to those in model (1); (iv) three tumour-present, immune-present states: (T^*, H_1^*, H_2^*, M_1^*, M_2^*). As an example, we illustrate these three tumour-immune coexistence states in Fig. E.18(a), as we vary parameter r_{M_1}, while keeping fixed $r_{M_2} = 0.05$, $a_{H_1} = 0.001$, $a_{H_2} = 0.001$, $g_{M_2} = 2.3 \times 10^{-10}$, $g_{H_1} = 5 \times 10^{-9}$ and all other parameters as in Table A.1. To have a better understanding of the immune responses during these three tumour sizes, in Figs. E.18(b), (c) we also plot the ratios of H_1^*/H_2^* and M_1^*/M_2^* corresponding to each of these three coexistence states. Note that for these tumour-immune states, the very low tumour sizes (described by squares in Fig. E.18(i)) occur in the presence of a type-I immune response (with $H_1/H_2 > 1$ in panel (ii), and $M_1/M_2 > 1$ in panel (iii)). In contrast, the very large tumour sizes occur in the presence of a type-II immune response.

Fig. E.19 shows the stability of all steady states exhibited by model (3), (including the coexistence states discussed previously), as we vary parameter r_{M_1} and keep all other parameters fixed.

References

Allavena, P., Mantovani, A., 2012. Immunology in the clinic review series; focus on cancer: tumour-associated macrophages: undisputed stars of the inflammatory tumour microenvironment. Clin. Exp. Immunol. 167, 195–205.

Almatroodi, S., McDonald, C., Darby, I., Pouniotis, D., 2016. Characterisation of M1/M2 tumour-associated macrophages (TAMs) and the Th1/Th2 cytokine profiles in patients with NSCLC. Cancer Micro. 9 (1), 1–11.

Asquith, B., Borghans, J., Ganusov, V., Macallan, D., 2009. Lymphocyte kinetics in health and disease. Trends Immunol. 30 (4), 182–189.

Barros, M., Hauck, F., Dreyer, J., Kempkes, B., Niedobitek, G., 2013. Macrophage polarisation: an immunohistochemical approach for identifying M1 and M2 macrophages. PLoS One 8 (11), e80908.

Benzekry, S., Lamont, C., Beheshti, A., Tracz, A., Ebos, J., Hlatky, L., Hahnfeldt, P., 2014. Classical mathematical models for description and prediction of experimental tumour growth. PLoS Comput. Biol. 10 (8), e1003800.

Bergmann, C., van Hemmen, J.L., Segel, L., 2001. Th1 or Th2: how an appropriate T helper response can be made. Bull. Math. Biol. 63, 405–430.

Boer, R.D., Person, A., 2013. Quantifying T lymphocyte turnover. J. Theor. Biol. 327, 45–87.

Borghans, J., De Boer, R.D., 2007. Quantification of T-cell dynamics: from telomeres to dna labeling. Immunol. Rev. 216 (1), 35–47.

Brown, J., Attardi, L., 2005. The role of apoptosis in cancer development and treatment response. Nat. Rev. Cancer 5, 231–237.

Burkholder, B., Huang, R., Burgess, R., Luo, S., Jones, V., Zhang, W., Lv, Z., Gao, C., Wang, B., Zhang, Y., Huang, R., 2014. Tumor-induced perturbations of cytokines and immune cells networks. Biochim. Et. Biophys. Acta 1845, 182–201.

Chen, P., Huang, Y., Bong, R., Ding, Y., Song, N., Wang, X., Song, X., Lou, Y., 2011. Tumor-associated macrophages promote angiogenesis and melanoma growth via adrenomedullin in a paracrine and autocrine manner. Clin. Cancer Res. 17 (23), 7230–7239.

Coussens, L., Werb, Z., 2002. Inflammation and cancer. Nature 420, 860–867.

Danciu, C., Falamas, A., Dehelean, C., Soica, C., Radeke, H., Barbu-Tudoran, L., Bojin, F., Pónzaru, S., Munteanu, M., 2013. A characterization of four b16 murine melanoma cell sublines molecular fingerprint and proliferation behavior. Cancer Cell Int. 13, 75. http://dx.doi.org/10.1186/1475-2867-13-75.

de Pillis, L., Radunskaya, A., Wiseman, C., 2005. A validated mathematical model of cell-mediated immune response to tumor growth. Cancer Res. 65 (17), 1916–1940.

den Breems, N., Eftimie, R., 2016. The re-polarization of M2 and M1 macrophages and its role on cancer outcomes. J. Theor. Biol. 390, 23–39.

DeNardo, D., Barreto, J., Andreu, P., Vasquez, L., Tawfik, D., Kolhatkar, N., Coussens, L., 2009. $CD4^+$ T cells regulate pulmonary metastasis of mammary carcinomas by enhancing protumor properties of macrophages. Cancer Cell 16, 91–102.

Eftimie, R., Bramson, J., Earn, D., 2010. Modeling anti-tumor Th1 and Th2 immunity in the rejection of melanoma. J. Theor. Biol. 265 (3), 467–480.

Eftimie, R., Gillard, J., Cantrell, D., 2016. Mathematical models for immunology: current state of the art and future research directions. Bull. Math. Biol. 78 (10), 2091–2134.

Ehrich, P., 1909. Ueber den jetzigen stand der karzinomforschung. Ned. Tijdschr. Geneeskd. 5, 73–290.

Fishman, M., Perelson, A., 1999. Th1/Th2 differentiation and cross-regulation. Bull. Math. Biol. 61, 403–436.

Flach, E., Schnell, S., 2006. Use and abuse of the quasi-steady-state approximation. Syst. Biol. 153 (4), 187–191.

Friberg, S., Mattson, S., 1997. On the growth rates of human malignant tumours: implications for medical decision making. J. Surg. Oncol. 65, 284–297.

Gauthier, E., Ivanov, S., Lesnik, P., Randolph, G., 2013. Local apoptosis mediates clearance of macrophages from resolving inflammation in mice. Blood 122 (15), 2714–2722.

Gliozzi, A., Guiot, C., Chignon, R., Delsanto, P., 2010. Oscillations in growth of multicelular tumour spheroids: a revisited quantitative analysis. Cell Prolif. 43 (4), 344–353.

Gross, F., Metzner, G., Behn, U., 2011. Mathematical modeling of allergy and specific immunotherapy: Th1-Th2-Treg interactions. J. Theor. Biol. 269 (1), 70–78.

Hanahan, D., Weinberg, R., 2011. Hallmarks of cancer: the next generation. Cell 144, 646–674.

Helming, L., 2011. Inflammation: cell recruitment versus local proliferation. Curr. Biol. 21 (14), R548–R550.

Heusinkveld, M., van der Burg, S., 2011. Identification and manipulation of tumour associated macrophages in human cancers. J. Transl. Med. 9, 216.

Hsieh, C., Macatonia, S., Tripp, C., Wolf, S., O'Garra, A., Murphy, K., 1993. Development of Th1 $CD4^+$ T cells through IL-12 produced by *Listeria*-induced macrophages. Science 260, 547–549.

Hung, K., Hayashi, R., Lafond-Walker, A., Lowenstein, C., Pardoll, D., Levitsky, H., 1998. The central role of $CD4^+$ T cells in the antitumor immune response. J. Exp. Med. 188 (12), 2357–2368.

Jenkins, S., Ruckerl, D., Cook, P., Jones, L., Finkelman, F., van Rooijen, N., MacDonald, A., Allen, J., 2011. Local macrophage proliferation, rather than recruitment from the blood, is a signature of Th2 inflammation. Science 332 (6035), 1284–1288.

Kim, Y., Lee, S., Kim, Y.-S., Lawler, S., Go, Y., Kim, Y.-K., Hwang, H., 2013. Regulation of Th1/Th2 cells in asthma development: a mathematical model. Math. Biosci. Eng. 10 (4), 1095–1133.

Knutson, K., Disis, M., 2005. Tumor antigen-specific T helper cells in cancer immunity and immunotherapy. Cancer Immunol. Immunother. 54 (8), 721–728.

Kogan, Y., Agur, Z., Elishmereni, M., 2013. A mathematical model for the immunotherapeutic control of the Th1/Th2 imbalance in melanoma. Discret. Contin. Dyn. Syst. Ser. B 18 (4), 1017–1030.

Kobayashi, M., Kobayashi, H., Pollard, R., Suzuki, F., 1998. A pathogenic role of Th2 cells and their cytokine products on the pulmonary metastasis of murine B16 melanoma. J. Immunol. 160, 5860–5873.

Laird, A., 1964. Dynamics of tumour growth. Br. J. Cancer 18 (3), 490–502.

Lamagna, C., Aurrand-Lions, M., Imhof, B., 2006. Dual role of macrophages in tumour growth and angiogenesis. J. Leukoc. Biol. 80 (4), 705–713.

Laydon, D., Bangham, C., Asquith, B., 2015. Estimating t cell repertoire diversity: limitations of classical estimators and a new approach. Philos. Trans. R. Soc. B 370 (1675), 20140291.

Lee, S., Starkey, P., Gordon, S., 1985. Quantitative analysis of total macrophage content in adult mouse tissues. J. Exp. Med. 161, 475–489.

Louzoun, Y., Atlan, H., Cohen, I., 2001. Modeling the influence of TH1- and TH2-type cells in autoimmune diseases. J. Autoimmun. 17 (4), 311–321.

Louzoun, Y., Xue, C., Lesinski, G., Friedman, A., 2014. A mathematical model for pancreatic cancer growth and treatments. J. Theor. Biol. 351, 74–82.

Lucey, D., Clerici, M., Shearer, G., 1996. Type 1 and type 2 cytokine dysregulation in human infectious, neoplastic, and inflammatory diseases. Clin. Microbiol. Rev. 9 (4), 532–562.

Magombedze, G., Eda, S., Ganusov, V., 2014. Competition for antigen between Th1 and Th2 responses determines the timing of the immune response switch during mycobaterium avium subspecies paratuberulosis infection in ruminants. PLOS Comput. Biol., 1–13.

Mantovani, A., Romero, P., Palucka, A., Marincola, F., 2008. Tumour immunity: effector response to tumour and role of the microenvironment. Lancet 371 (9614), 771–783.

Martinez, F.O., Gordon, S., 2014. The M1 and M2 paradigm of macrophage activation: time for reassessment.. F1000Prime Reports., 6–13.
Mattes, J., Hulett, M., Xie, W., Hogan, S., Rothenberg, M., Foster, P., Parish, C., 2003. Immunotherapy of cytotoxic T cell-resistant tumors by T helper 2 cells: an eotaxin and STAT6-dependent process. Exp. Med 197 (3), 387–393.
Mills, C., Ley, K., 2014. M1 and M2 macrophages: the chicken and the egg of immunity. J. Innate Immun. 6 (6), 716–726.
De Monte, L.D., Reni, M., Tassi, E., Clavenna, D., Papa, I., Recalde, H., Braga, M., Di Carlo, V., Doglioni, C., Protti, M., 2011. T helper type 2 cell infiltrate correlates with cancer-associated fibroblast thymic stromal lymphopoietin production and reduced survival in pancreatic cancer. J. Exp. Med. 208, 469–478.
Moore, H., Li, N., 2004. A mathematical model for chronic myelogenous leukaemia (CML) and T cell interactions. J. Theor. Biol. 227, 513–523.
Murphy, H., Jaafari, H., Dobrovolny, H., 2016. Differences in predictions of ODE models of tumor growth: a cautionary example. BMC Cancer 16, 163.
N.I.H., O.A.C.U., Guidelines for endpoints in animal study proposals, ⟨http://oacu.od.nih.gov/ARAC/documents/ASPEndpoints.pdf⟩ (1996).
Panzer, M., Sitte, S., Wirth, S., Drexler, I., Sparwasser, T., Voehringer, D., 2012. Rapid in vivo conversion of effector T cells into Th2 cells during helminth infection. J. Immunol. 118 (2), 615–623.
Preuße, C., Goebel, H., Held, J., Wengert, O., Scheibe, F., Irlbacher, K., Koch, A., Heppner, F., Stenzel, W., 2012. Immune-mediated necrotizing myopathy is characterized by a specific Th1-M1 polarized immune profile. Am. J. Pathol. 181 (6), 2161–2171.
Protti, M., DE Monte, L.D., 2012. Cross-talk within the timor microenvironment mediates Th2-type inflammation in pancreatic cancer. OncoImmunology 1, 89–91.
Roberts, C., Dickinson, A., Taams, L., 2015. The interplay between monocytes/macrophages and $CD4^+$ T cell subsets in rheumatoid arthritis. Front. Immunol. 6, 571.
Romagnani, S., 1999. Th1/Th2 cells. Inflamm. Bowel Dis. 5 (4), 285–294.
Sarapata, E., de Pillis, L., 2014. A comparison and catalog of intrinsic tumour growth models. Bull. Math. Biol. 76, 2010–2024.
Severins, M., Broughams, J., de Boer, R., 2008. The role of Th1/Th2 phenotypes in T cell vaccination: insights from a mathematical model. In: T-cell vaccination, Nova Science Publishers, Inc., pp. 139–158.
Sica, A., Larghi, P., Mancino, A., Rubino, L., Porta, C., Totaro, M., Rimoldi, M., Biswas, S., Allavena, P., Mantovani, A., 2008. Macrophage polarization in tumour progression. Semin. Cancer Biol. 18 (5), 349–355.
Solinas, G., Germano, G., Mantovani, A., Allavena, P., 2009. Tumour-associated macrophages (TAM) as major players of the cancer-related inflammation. J. Leukoc. Biol. 86, 1065–1073.
Talkington, A., Durrett, R., 2015. Estimating tumour growth rates in vivo. Bull. Math. Biol. 77, 1934–1954.
Tatsumi, T., Kierstead, L., Ranieri, E., Gesualdo, L., Schena, F., Finke, J., Bukowski, R., Mueller-Berghaus, J., Kirkwood, J., Kwok, W., Storkus, W., 2002. Disease-associated bias in T helper type 1 (Th1)/Th2 $CD4^+$ T cell responses against MAGE-6 in HLA-$DRB1^*0401^+$ patients with renal cell carcinoma or melanoma. J. Exp. Med 196 (5), 619–628.
Taylor-Robinson, A., 1997. Inhibition of IL-2 production by nitric oxide: a novel self-regulatory mechanism for Th1 cell proliferation. Immunol. Cell Biol. 75, 167–175.
Voena, C., Chiarle, R., 2016. Advances in cancer immunology and cancer immunotherapy. Discov. Med. 21 (114), 125–133.
Wang, Y., Yang, T., Ma, Y., Halade, G., Zhang, J., Lindsey, M., Jin, Y.-F., 2012. Mathematical modeling and stability analysis of macrophage activation in left ventricular remodeling post-myocardial infarction. BMC Genom. 13, S21.
Wang, M., Yin, B., Wang, H., Wang, R., 2014. Current advances in t-cell-based cancer immunotherapy. Immunotherapy 6 (12), 1265–1278.
Wang, Q., Klinke, D., Wang, Z., 2015. $CD8^+$ T cell response to adenovirus vaccination and subsequent suppression of tumor growth: modeling, simulation and analysis. BMC Syst. Biol. 9, 27.
Weisser, S., McLarren, K., Kuroda, E., Sly. L., 2013, Methods in molecular biology: Generation and characterisation of murine alternatively activated macrophages. 946 225-239.
Wigginton, J., Kirschner, D., 2001. A model to predict cell-mediated immune regulatory mechanisms during human infection with *Mycobacterium tuberculosis*. J. Immunol. 166, 1951–1967.
Wodarz, D., Iwasa, Y., Komarova, N., 2004. On the emergence of multifocal cancers. J. Carcinog. 3, 13.
Wong, R., 2011. Apoptosis in cancer: from pathogenesis to treatment. J. Exp. Clin. Res. 30, 87.
Xie, Y., Akpinarli, A., Maris, C., Hipkiss, E., Lane, M., Kwon, E., Muranski, P., Restifo, N., Antony, P., 2010. Naive tumor-specific $CD4^+T$ cells differentiated in vivo eradicate established melanoma. J. Exp. Med. 207 (3), 651–667.
Yamaguchi, T., Fushida, S., Yamamoto, Y., Tsukada, T., Kinoshita, J., Oyama, K., Miyashita, T., Tajima, H., Ninomiya, I., Munesue, S., Harashima, A., Harada, S., Yamamoto, H., Ohta, T., 2016. Tumor-associated macrophages of the M2 phenotype contribute to progression in gastric cancer with peritoneal dissemination. Gastric Cancer 19 (4), 1052–1065.
Yates, A., Bergmann, C., Hemmen, J.V., Stark, J., Callard, R., 2000. Cytokine-modulated regulation of helper T cell population. J. Theor. Biol. 206 (4), 539–560.
T. Yu, Design and validation of a mathematical model to describe macrophage dynamics in wound healing, Master's thesis, Drexel University (2014).
Zhang, M., He, Y., Sun, X., Li, Q., Wang, W., Zhao, A., Di, W., 2014. A high M1/M2 ratio of tumour-associated macrophages is associated with extended survival in ovarian cancer patients. J. Ovarian Res. 7, 19.
Zhu, J., Guo, L., Min, B., Watson, C., Hu-Li, J., Young, H., Tsichlis, P., Paul, W., 2002. Growth factor independent-1 induced by IL-4 regulates Th2 cell proliferation. Immunity 16 (5), 733–744.